Environmental Nanotechnology, Monitoring & Management 18 (2022) 100737

Contents lists available at ScienceDirect

Environmental Nanotechnology, Monitoring & Management

journal homepage: www.elsevier.com/locate/enmm

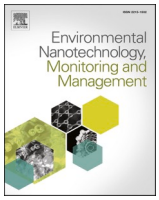

Efficient photocatalysis of carbon coupled TiO_2 to degrade pollutants in wastewater – A review

Charitha Thambiliyagodage

Faculty of Humanities and Sciences, Sri Lanka Institute of Information Technology, New Kandy Road, Malabe, Sri Lanka

ARTICLE INFO

Keywords:
TiO_2
Activated carbon
Carbon nanotubes
Graphene
g-C_3N_4
Photocatalysis

ABSTRACT

Water pollution caused by human activities is a monumental problem that the world is facing today. The use of polluted water for domestic, industrial, and agricultural applications creates severe hazardous issues. Therefore, decontamination of polluted water is greatly important. The advanced oxidation process is preferred to purify contaminated water as the pollutants are completely degraded to harmless products. TiO_2 is the most widely researched photocatalyst due to its chemical stability, low cost and eco-friendliness. However, the use of TiO_2 is limited as it is only sensitive to UV range due to its high band gap (3.0 eV for rutile) and the possible electron-hole pair recombination. TiO_2 has been coupled with carbon-based materials to enhance photocatalytic activity by enhancing charge separation and visible light absorption. This review summarizes the recent use of TiO_2 coupled to activated carbon, carbon nanotubes, graphene derivatives, and g-C_3N_4 to degrade different pollutants found in water including dyes, pesticides, pharmaceuticals, phenols and heavy metals. The advantages and disadvantages of using each carbon-based material are discussed. Further, the challenges and opportunities associated with all the materials are presented. Finally, recommendations and possible future outlooks are briefed in this review.

1. Introduction

Water scarcity is a major problem that needs to be addressed with great importance as all living beings are immensely affected. Water contamination is mainly caused by rapid industrialization which releases many hazardous chemicals including but not limited to heavy metals (Chai et al., 2021), dyes (Thambiliyagodage, 2021), pesticides (Saleh et al., 2020), fertilizers (Xiaojing Zhang et al., 2021), pharmaceuticals (Xiaojing Zhang et al., 2021). Mixing such chemicals into normal water reservoirs causes harmful effects as the pollutants are highly toxic, chemically stable, less biodegradable, and high recalcitrance, and hence they tend to accumulate in the environment (Rashid et al., 2021; Wong et al., 2019) Therefore, certainly they need to be removed from contaminated water. There are different techniques available for wastewater purification including physical methods such as adsorption (N. Cheng et al., 2021; Usgodaarachchi et al., 2021), coagulation/flocculation (Luo et al., 2019), membrane filtration (P. Li et al., 2021), nanofiltration (Cao et al., 2021), precipitation(M. Kumar et al., 2021), chemical methods like oxidation (D. Ma et al., 2021), and biological methods including remediation by microorganisms (P. Sharma et al. (2021a)) and enzymes (Al-Maqdi et al., 2021)etc. However, collectively these techniques possess different disadvantages including incomplete removal of the pollutants, concentration to another phase, especially in adsorption, precipitation and filtration, low efficiency and increased processing time, high cost associated with installation and running cost, low durability, high selectivity, production of toxic byproducts etc (Rashid et al., 2021; Wong et al., 2019). Among them, advanced oxidation has become an emerging widely applicable technique as it degrades the pollutants into harmless products completely.

The advanced oxidation process involves a semiconductor that could be excited by light with an energy higher than its band gap to produce electrons and holes which lead to the production of radicals that degrade the pollutant molecules. The light source could be either UV light, visible light, UV-Visible light or simply sunlight which is a sustainable and renewable energy source. Widely researched semiconductors are metal oxides such as TiO_2 (Paumo et al., 2021), ZnO (El Golli et al., 2021), CeO_2 (J. Hu et al., 2022), WO_3 (M. Liao et al., 2021), $SrTiO_3$ (Q. Zhou et al., 2022), metal sulfides like CdS (Devendran et al., 2022), ZnS (Xaba, 2021), WS_2 (Barakat et al., 2022), Bi_2S_3(Tao et al., 2022) and even metal nitrides including Ta_3N_5 (Akter, Hanif, Islam, Sapkota, Lee, et al., 2021), Si_3N_4 (S. Wang et al., 2021)etc. Among them, TiO_2 is the

E-mail address: charitha.t@sliit.lk.

https://doi.org/10.1016/j.enmm.2022.100737
Received 17 April 2022; Received in revised form 14 July 2022; Accepted 24 August 2022
Available online 27 August 2022

most studied semiconductor due to its high stability, low cost and eco-friendliness (Gupta & Tripathi, 2011). The main drawback of using TiO_2 as the semiconductor is its wide ban gap (rutile – 3.0 and anatase 3.2 eV) where UV irradiation is required to excite an electron from the valence band (VB) to the conduction band (CB) (Hanaor & Sorrell, 2011; X. J. Yang et al., 2015). Various strategies have been implemented to increase the visible light absorption of TiO_2. Narrowing of the band gap and hence the visible light sensitivity has been achieved by doping with metals like Fe (Thambiliyagodage & Mirihana, 2021), Cu (Mathew et al., 2018), Mn (Prashad Ojha et al., 2020), Ag (T. Ali et al., 2018)etc., with non-metals such as N (J. Huang et al., 2021), C (Varnagiris et al., 2019), S (Piątkowska et al., 2021)etc. with both metals and non-metals including Fe-N (Thambiliyagodage & Usgodaarachchi, 2021), Cu-S (Haris et al., 2019) etc. Further, TiO_2 has been coupled with other semiconductors such as WO_3 (Balayeva et al., 2018), CuO (Edelmannová et al., 2018), and Fe_2O_3 (Fawzi Suleiman Khasawneh and Palaniandy, 2021) etc. to improve the photocatalytic activity upon irradiation with the visible irradiation. Further, different strategies including hybridization with narrow optical gap semiconductors, bandgap engineering, upconversion materials, plasmonic materials, and photosensitizers have been reported to enhance the near infra-red capture by TiO_2 based photocatalysts increasing the overall solar spectrum utilization (L. Jiang et al., 2022). The main disadvantage of TiO_2 coupling with the metal oxides is the requirement of proper band alignment. For example, type II band alignment favours the electron-hole pair separation while type I band alignment causes charge recombination(Thambiliyagodage, 2021). TiO_2 coupled with non-metal oxides have exhibited enhanced photocatalytic activity.

In this review, we summarized the recently published research papers on photocatalysis of TiO_2 coupled with carbon-based materials including activated carbon, g-C_3N_4, carbon nanotubes, and graphene oxide, advantages and disadvantages associated with coupling with each material and the challenges and opportunities, research gaps, recommendations, and future perspectives. Here, we report the findings of recent research papers. Hence, we believe that this review article would be advantageous to all the readers who are researching photocatalysis, semiconductors, environmental remediation, adsorption etc.

2. TiO_2/carbon-based materials

2.1. UV/UV-visible active TiO_2/Carbon-based materials

2.1.1. TiO_2/activated carbon (AC)

2.1.1.1. Degradation of pollutants. The effect of an activating agent on the activation of carbon and such effect on photocatalytic activity was determined on photodegradation of acetaminophen (ACE) in the presence of TiO_2/AC(Manuel Peñas-Garzón et al., 2019). $FeCl_3$, $ZnCl_2$, H_3PO_4 and KOH have been used as the activating agents to activate lignin, maintaining the active agent to lignin mass ratio of 3:1 except with KOH where it was kept at 4:1. $ZnCl_2$ and H_3PO_4 are known to activate carbon mainly via dehydration of lignin during the heat treatment. H_3PO_4 is a strong Bronsted acid that causes partial depolymerization of lignin followed by dehydration and condensation. $ZnCl_2$ is a Lewis acid and the reaction with lignin is proton catalyzed resulting in dehydration and aromatization of the carbon skeleton (Caturla et al., 1991). KOH reacts with lignin via oxidation and reduction reactions producing highly microporous carbon developed after oxidizing carbon to CO and CO_2. A similar microporosity development has been observed with $FeCl_3$ activation(Bedia et al., 2018). TiO_2/AC was synthesized by solvothermal where the TiO_2 to AC ratio was maintained at 4:1 and the respective heterostructures synthesised are denoted as TiO_2/Fe-C, TiO_2/Zn-C, TiO_2/P—C and TiO_2/K-C. According to the SEM images particles of bare TiO_2 and the heterostructures are spherical and as shown in the histograms (Fig. 1) particle size of the heterostructures are in the range of 0.24–0.28 μm and are lower than that of bare TiO_2 (0.351 μm)

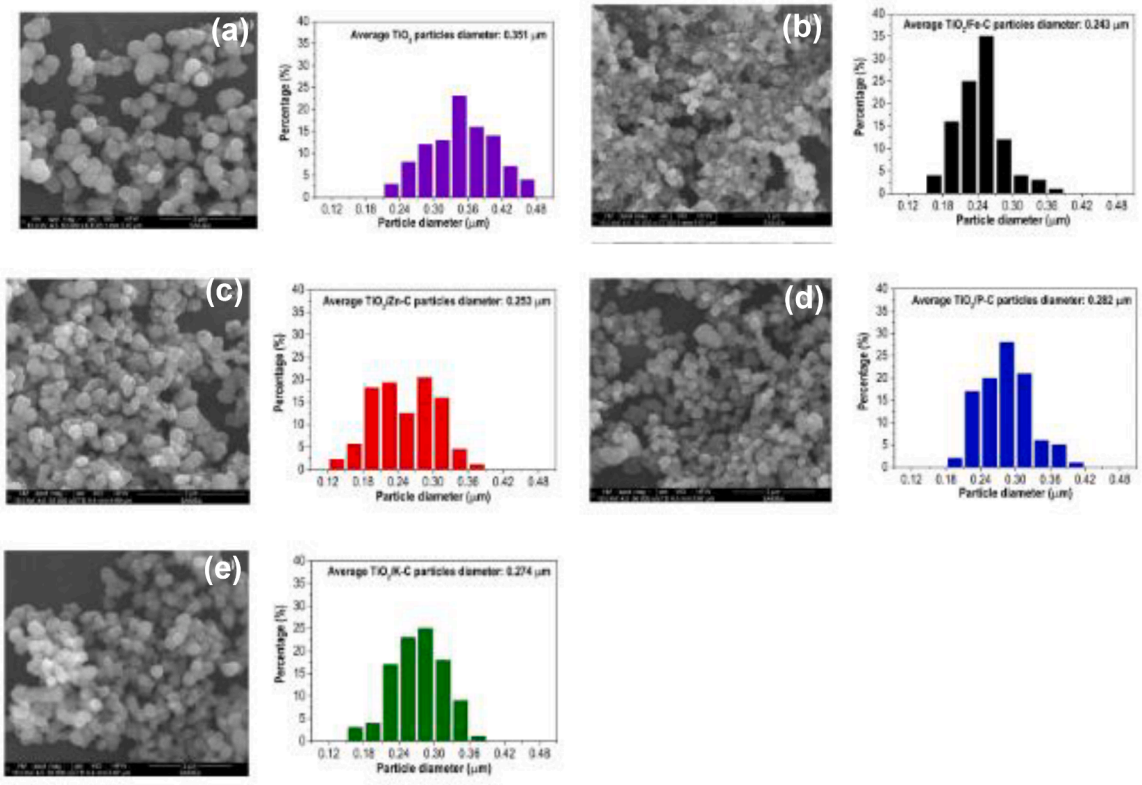

Fig. 1. SEM images and particle size distribution of (a) TiO_2 (b) TiO_2/Fe-C (c)TiO_2/Zn-C (d) TiO_2/P—C and (e) TiO_2/K-C. Figure adapted from ref.(Manuel Peñas-Garzón et al., 2019).

indicating that presence of AC inhibits the particle growth (Xiaojing Wang et al., 2009). The specific surface area of AC prepared by using KOH has shown the highest (1446 m^2/g) while the least has resulted with carbon activated by $FeCl_3$ (756 m^2/g). TiO_2/Zn-C exhibited the highest specific surface area (491 m^2/g), while the lowest was obtained with TiO_2/Fe-C (300 m^2/g). It was observed that after 16 h of keeping the samples in dark, bare TiO_2 showed the highest photocatalytic activity due to the easy accessibility and higher opacity created by the black-grey colour of the heterostructures. Among the heterostructures synthesized TiO_2/Fe-C showed the highest photocatalytic activity due to the lowest band gap of this photocatalyst. TOC also supported the above observation that after 6 h of complete conversion of acetaminophen, bare TiO_2 removed 59.4 % of TOC being the highest and TiO_2/Fe-C removed 43.3 % TOC while the least % removal of TOC was obtained from TiO_2/Zn-C. However, TiO_2/Fe-C was able to settle faster than bare TiO_2, suggesting that TiO_2/Fe-C was easy to recover from the medium which is a key parameter used in selecting the best catalyst. Further, there was no significant reduction in the photocatalytic activity of TiO_2/Fe-C after four successive cycles.

TiO_2/AC composites synthesized by solvothermal (ST), microwave-assisted (MW), and sol–gel synthesis (SG) routes were evaluated for their photocatalytic activity on degradation of acetaminophen (ACE), ibuprofen (IBU) and anti-pyrine (ANT) under simulated solar light(M. Peñas-Garzón et al., 2020). AC has been prepared via the $FeCl_3$ activation pathway (Bedia et al., 2017, 2018; Zazo et al., 2012) where the mixture of lignin and $FeCl_3$ was heat-treated at 800 °C in the N_2 atmosphere followed by leaching in HCl to remove the excess activating agent and then was rinsed with ultrapure water till pH become neutral. TiO_2 and AC was mixed in a mass ratio of 4:1 to prepare the composite (Manuel Peñas-Garzón et al., 2019). TiO_2 particles of anatase phase with mean particle sizes of 0.32, 0.27 and 0.24 μm, respectively, in TiO_2/AC-SG, TiO_2/AC-MW and TiO_2/AC-ST were distributed on AC. Band gap values calculated by UV-Visible diffuse reflectance spectroscopy were 3.28, 3.35, and 3.38 eV, while the specific surface areas of those composites were 130, 323, and 300 m^2/g, respectively. Composites were kept in dark for 16 h to reach the adsorption-desorption equilibrium where the adsorption followed pseudo second-order kinetics. Though TiO_2/AC-MW and TiO_2/AC-ST showed similar activity in degradation of ACE, which was almost completed by 4 h, only a 50 % of reduction in the concentration of ACE was obtained by TiO_2/AC-SG due to its low porosity and high particle size (Fig. 2(a)). Meanwhile, according to the percentage removal of TOC as shown in the inset of Fig. 2(a), the highest mineralization (47 %) has resulted in the presence of TiO_2/AC-MW. As there were no significant changes in the intensity of the photoluminescence spectra it is evident that the photocatalytic activity was predominantly affected by the structural and textural properties and not by a contribution of the charge recombination rate. TiO_2/AC-MW and TiO_2/AC-ST were effective in the mineralization of IBU but not ANT successfully (Fig. 2(b) and (c), respectively). When the values of the first-order kinetic constants were considered the effectiveness of TiO_2/AC-MW on the disappearance of the pharmaceuticals has been varied as IBU > ACE > ANT. However, the absorptivity of these pharmaceuticals to

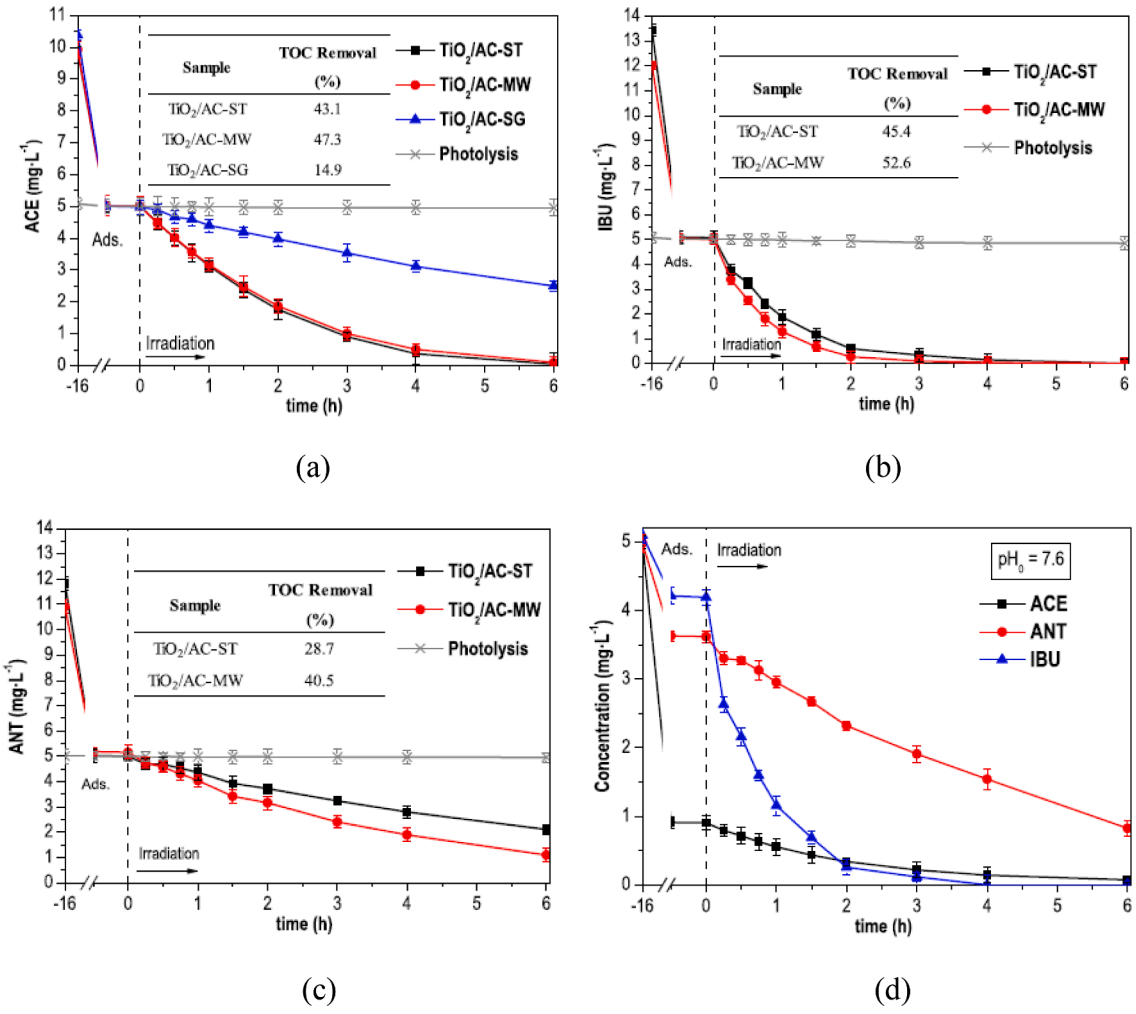

Fig. 2. Adsorption and solar photocatalytic degradation of (a) ACE (b) IBU (c) ANT separately, and (d) all three in a mixture. Figure adapted from ref.(M. Peñas-Garzón et al., 2020).

TiO_2/AC-MW was varied as ACE ≫ ANT > IBU being different to what resulted with single compounds, but the photocatalytic activity was similar to that resulting with the individual compounds (Fig. 2(d)). Though complete mineralization was achieved after 24 h the TOC remained unchanged (50 %), indicating the presence of byproducts. As the study has elaborated to determine the effect of pH in the medium on adsorption and photocatalytic activity it has been observed that IBU is completely adsorbed at pH ≤ 5, whereas its adsorption decreased at alkaline pH due to the electrostatic repulsions between IBU ($pK_a = 4.4$) and the catalyst surface ($pH_{PZC} = 7.0$). The photodegradation of ACE decreased with increasing pH, while it increased for ANT, showing the highest activity for ANT compared to the others. Activity on IBU at low pH values could not be determined due to the complete adsorption of IBU to the catalyst surface (M. Peñas-Garzón et al., 2020).

TiO_2 coupled with AC is photo catalytically active in the degradation of RhB under UV light(Xing et al., 2016). AC was prepared using lignite as the raw material via the KOH activation pathway where KOH was mixed with lignite in a weight ratio of 2:1 and annealed at 800 °C for 2 h in a N_2 atmosphere. Obtained AC with a specific surface area of 1576 m^2/g and a pore volume of 0.967 cm^3/g was mixed with TiO_2 sol prepared by sol–gel synthesis using $Ti(OC_4H_9)_4$ as the titanium precursor, in different TiO_2 loadings as 1,2 and 3 (TiO_2/AC-1, TiO_2/AC-2 and TiO_2/AC-3, respectively). Obtained composite has been annealed at 500 °C for 3 h in a N_2 flow. Produced anatase TiO_2 has been coupled with amorphous AC, where the specific surface area, micropore surface area, mesopore surface area, total pore volume etc. decrease with increasing TiO_2 loading because the more the TiO_2 deposited more the micropores get blocked. TiO_2 nanoparticles were deposited not only surface of AC but also on the mesopores and macropores without any significant agglomeration which will increase the probability of receiving light and hence increase the photocatalytic activity (Xue et al., 2011). Moreover, though nanoparticles were dispersed at low TiO_2 loading (TiO_2/AC-1 and TiO_2/AC-2) nanoparticles tend to agglomerate with increasing TiO_2 content TiO_2/AC-3. The photocatalytic activity of the synthesized composites was determined by the photodegradation of RhB under the exposure of irradiation generated by a 450 W high pressure mercury lamp. Before exposure to the UV irradiation, RhB solutions (400 mL of 2×10^{-5} mol/L) with the composites were stirred in dark for 90 min to reach the adsorption-desorption equilibrium. AC removed 71.0 % RhB by adsorption during the 90 min in dark and showed no degradation after exposing to UV light, while, though the removal of RhB by TiO_2 by adsorption in dark is negligible, upon exposure to UV light, 55.8 % of RhB was photodegraded. However, TiO_2/AC composites removed RhB more efficiently than both AC and TiO_2 which was attributed to both adsorption and photodegradation (C. Gu & Shannon, 2007; S. G. Kumar & Devi, 2011). Totally, 82.0 %, 93.2 % and 86.3 % of RhB was removed by TiO_2/AC-1, TiO_2/AC-2 and TiO_2/AC-3, respectively, where 15.9 %, 46.5 % and 47.4 % RhB was photodegraded in the presence of the respective photocatalysts (Fig. 3(a and b)). Among the photocatalysts, TiO_2/AC-2 has exhibited the highest photocatalytic activity compared to the loading of TiO_2. When photocatalytic activity is considered adsorption of the dye molecules before photodegradation is crucial (Lim et al., 2011; Omri & Benzina, 2014). The presence of AC allows the adsorption of RhB which facilitates the photodegradation as the $OH^{\cdot}$ and $O_2^{\cdot-}$ produced by the photogenerated electrons and holes, respectively, are in proximity to the RhB molecules. The removal efficiency was predominated by adsorption in TiO_2/AC-1 due to the presence of a high amount of AC with many adsorption sites. Photocatalytic activity of TiO_2/AC-3 was lower compared to the loading of TiO_2 due to the aggregation of nanoparticles and the reduction of the porosity. Therefore, it is evident that both the porosity and the dispersibility are the crucial parameters in obtaining high photocatalytic activity (Xing et al., 2016).

Wang et al. reported the effect of calcination temperature on the photocatalytic activity of TiO_2/AC composites synthesized by the sol-gel synthesis method using $Ti(OC_3H_7)_4$ as the titanium precursor and commercial AC (Darco G-60, 100 mesh Aldrich (W. Wang et al., 2007). Composites have been prepared varying the initial AC weight to final TiO_2 weight as 20, 50 and 80 and the annealing temperature as 300, 450 and 600 °C. It was observed that the specific surface area increased with the increasing weight of AC in the composite, while it decreased with increasing calcination temperature. The rate constant for the degradation of Chromotrope 2R under UV light decreased with increasing calcination temperature regardless of the weight of AC. Further, the apparent first order rate constant and hence the photocatalytic activity decreased with increasing initial Chromotrope 2R concentration. The surface area has not been considered the only factor which contributes to photocatalysis as even with lower surface areas high-rate constants have resulted. Photosensitizer effect may also have contributed to the photocatalytic activity where the photoexcited organic molecules which are previously adsorbed to the AC surface inject electrons to the conduction band of TiO_2 and enhance the formation of superoxide ion, $O_2^{\bullet-}$. These ions are also formed by subsequent electron transfer to molecular oxygen adsorbed to AC (Lettmann et al., 2001). Moreover, AC can also serve as a photosensitizer where they also transfer electrons to the

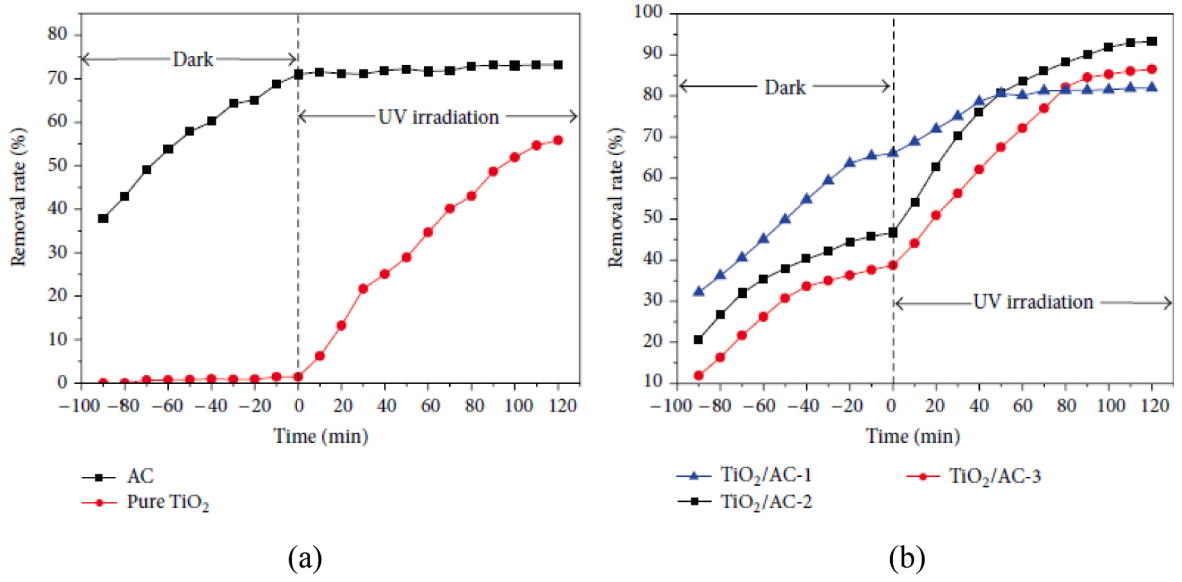

Fig. 3. RhB removal rate of (a) pure TiO_2 and AC, (b) TiO_2/AC composites. Figure adapted from ref. (Xing et al., 2016).

semiconductors and enhance the radical formation which eventually degrades the organic molecules(Nasr et al., 1996; W. Wang et al., 2007).

Martins et al. reported the synthesis of TiO_2/AC composites using the sol-gel method and their photocatalytic activity on degrading Tetracycline (A. C. Martins et al., 2017). AC was prepared by activating macadamia nut shells with NaOH and titanium isopropoxide was used as the titanium precursor where hydrolysis of the precursor was performed in the presence of AC in the medium. Mesoporous TiO_2/AC with a surface area of 129 m^2/g shows anatase polymorphic crystal structure and a band gap of 3.04 eV. It was photocatalytically active in the degradation of tetracycline under UV light generated by 18 W germicide lamp. TiO_2/AC showed the highest rate constant for the degradation of tetracycline (42.9×10^{-3} min^{-1}) which is greater than that of P25 which is 35.3×10^{-3} min^{-1} due to the lowered band gap, the high surface area which provides a greater interface between the tetracycline molecules and the catalyst surface, and decrease in the charge recombination at TiO_2 (Leary & Westwood, 2011; A. C. Martins et al., 2017; Mutuma et al., 2015; Slimen et al., 2011).

Fu et al. reported the effectiveness of the TiO_2/AC on adsorptive and photocatalytic removal of Cr(VI) once the surface of AC is functionalized by diethylenetriamine (DETA)(Fu et al., 2015). $Ti(C_4H_9O)_4$ was used as the titanium precursor and a combination of sol-gel synthesis and solvothermal methods was used for the synthesis. The surface of the AC was oxidized by treating the TiO_2/AC with HNO_3 and the carboxylic acid groups introduced during oxidation were transformed into acid chloride groups by treating with $SOCl_2$. DETA was attached to such activated AC surface via amidation AC-$COCl_2$ groups and NH_2 of DETA. The mechanism is shown in Scheme 1. Cr(VI) was adsorbed to the adsorbents in the order of AC-DETA > TiO_2/AC-DETA > AC > TiO_2/AC > TiO_2 as shown in Fig. 4(a). It could be seen that the presence of TiO_2 reduces the adsorption of DETA as the AC surface is covered with TiO_2 particles and hence the available surface to get functionalized and then adsorb Cr(VI) is lower when the same weight was considered. Adsorption data were well fitted to pseudo second order kinetics indicating the chemisorption of Cr(VI) and was fitted to Langmuir isotherm suggesting monolayer adsorption(Q. Yu et al., 2008). Cr(VI) which exists as $HCrO_4^-$ in a low pH medium (S. H. Huang & Chen, 2009) could form chemical interactions with the TiO_2/AC-DETA via electrostatic attractions occur between the positively charged amino groups and negatively charged $HCrO_4^-$, coordinative interactions between the Cr atoms and the N atoms and hydrogen bonding occur between the H atoms of the amino groups and the O atoms of $HCrO_4^-$. Photocatalytic activity of the synthesized materials was determined upon exposure to a 300 W mercury lamp with major emission at 365 nm. As exhibited in Fig. 4(b) AC and AC-DETA were photocatalytically inactive and the photoreduction of Cr(VI) to Cr(III) by the other materials showed, that TiO_2/AC-DETA > TiO_2/AC >

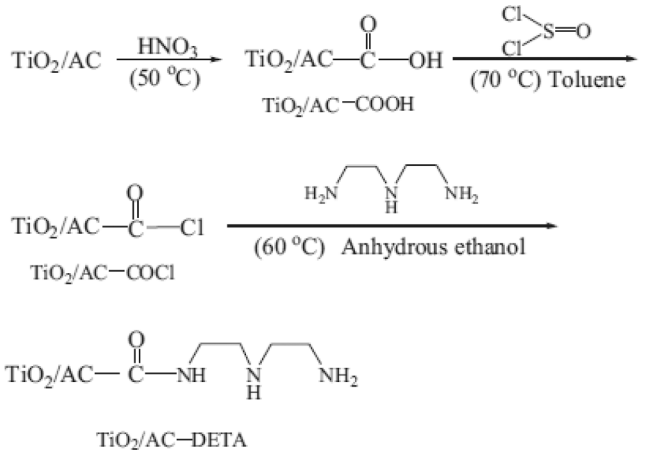

Scheme 1. Mechanism of amidation of AC surface of TiO_2/AC. Scheme adapted from ref. (Fu et al., 2015).

TiO_2 and the rate constant for the photoreduction in the presence of TiO_2/AC-DETA was 4.5 and 6.2 times of that TiO_2/AC and TiO_2, respectively. Further, the adsorption in dark followed by photocatalytic activity of TiO_2/AC-DETA and TiO_2/AC did not significantly drop after 5 cycles. The high photocatalytic activity of TiO_2/AC-DETA has been attributed to the proposed factors of (1) effective mass transfer of Cr(VI) to the AC surface from the bulk solution due to the surface functionalization (2) facilitated transfer of Cr(VI) from AC to TiO_2 and the migration of photogenerated electrons from TiO_2 to AC which has been attributed to the formation of interface junction between AC and TiO_2 and lastly the photoreduction of Cr(VI) at TiO_2 and AC. The possible overall process of photoreduction of Cr(VI) to Cr(III) is illustrated in scheme 2(Fu et al., 2015).

Further, TiO_2/AC has been reported to be effective in adsorbing and photodegrading tartrazine (Andriantsiferana et al., 2014), methyl orange (Xiaojing Wang et al., 2009), phenol (Tryba et al., 2003), humic acid (Xue et al., 2011) pharmaceuticals, amoxicillin, ampicillin, diclofenac and paracetamol (Gar Alalm et al., 2016) etc.

Guo *et al.* (Guo et al., 2021) reported the adsorptive and photocatalytic removal of 2-Methylisoborneol (2-MIB) which is a common taste and odour compound found in drinking water. Commercially available powdered activated carbon (PAC) was functionalized with 10 % HCl and was coupled with TiO_2 during the sol-gel synthesis. Adsorptive removal of 2-MIB by PAC (~97 %) was higher than TiO_2/PAC (~90 %) because of blockage of mesopores and micropores due to the diffusion of TiO_2 which further decrease the surface area. Adsorption followed the Freundlich isotherm model suggesting that the adsorption sites were non-uniformly distributed and 2-MIB molecules adsorb as multilayers to the adsorbents. TiO_2/PAC and PAC degrade 2-MIB under UV irradiation. PAC removed 49.4 % of 2-MIB while TiO_2/PAC removed only 35.3 % from aqueous solutions in dark. During the exposure to light, TiO_2/PAC degrade 97.8 % of 2-MIB and 65.4 % of 2-MIB was removed by PAC. The rate of photodegradation of 2-MIB (16.8×10^{-3} min^{-1}) was 9 times greater than resulting in the presence of PAC (1.85×10^{-3} min^{-1}) due to the increase in dissociation of the functional groups in TiO_2/PAC by the chain scission and oxidation by UV radiation which made more available adsorption cites on TiO_2/PAC (Guo et al., 2021). Briche *et al.* reported the adsorptive and photodegradative removal of sulfamethazine in the presence of TiO_2/AC which is a common pharmaceutical found in wastewater. TiO_2/AC composites were synthesized by the sol-gel method in different molar ratios of titanium to AC in the range of 1/10 to 7/10. Freundlich isotherm model was followed suggesting that the sulfamethazine adsorb to TiO_2/AC as multilayers. Further, 94 % of sulfamethazine was photodegraded efficiently (0.025 min^{-1}) in the presence of TiO_2/AC prepared with the molar ratio of 0.5 under UV light produced by UVA lamps (27 W) (Briche et al., 2020). Recently, modified TiO_2/AC composites for efficient removal of pollutants from the environment were reported. Magnetic photocatalysts prepared using AC, TiO_2 and iron nitrate are found to effectively remove Reactive Black from an aqueous medium via adsorption and photocatalysis. Maximum TiO_2loaded magnetic AC removed 95 % of the dye totally, of which 67 % is due to photodegradation while the remaining 28 % of the dye was removed by adsorption. Magnetism created by adding iron nitrate and hence producing Fe_3O_4 enhanced the percent recovery of the catalyst which decreased with the increasing proportion of TiO_2 (de Oliveira Pereira et al., 2019). Therefore, it is evident that TiO_2 coupled to AC is a novel and effective composite in removing pollutants via adsorption and photodegradation. Table 1 summarizes the synthesis method, textural and optical parameters along with the photocatalysis of TiO_2/AC reported in the literature.

2.1.1.2. Advantages and disadvantages. TiO_2 particles tend to agglomerate during the synthesis and when they are supported on AC they appear to be well dispersed resulting in high photocatalytic activity. One disadvantage associated with TiO_2 is the recombination of electron hole

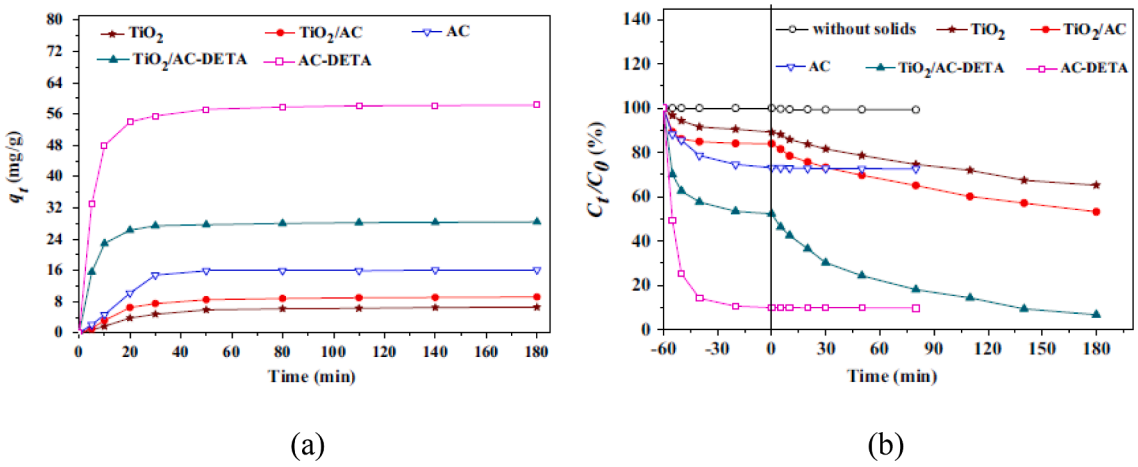

Fig. 4. (a) Adsorption kinetics of Cr(VI) (b) Adsorption and photoreduction of Cr(VI) (the vertical line at time t = 0 separates the dark period from the UV irradiation. Figure adapted from ref. (Fu et al., 2015).

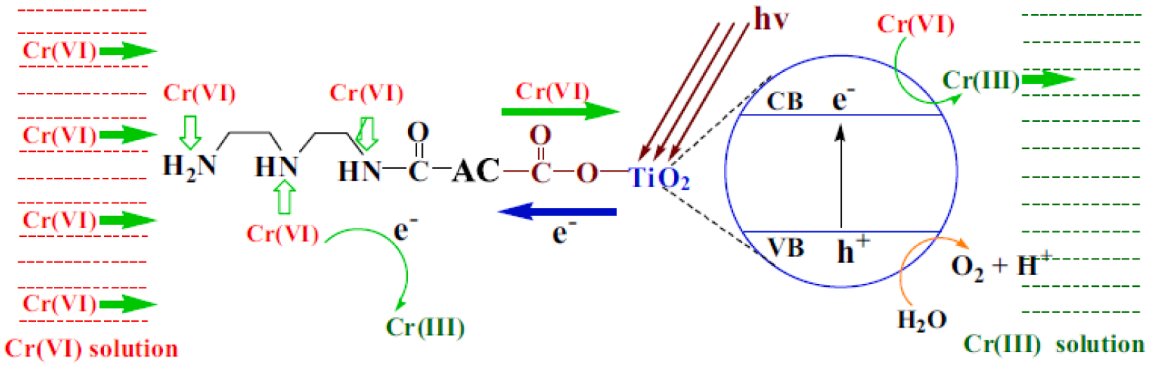

Scheme 2. The possible overall process of photoreduction of Cr(VI) to Cr(III). Scheme adapted from ref. (Fu et al., 2015).

pairs which leads to low photocatalytic activity. Once they are immobilized on AC photogenerated electrons are trapped by AC and pass to the molecules of interest limiting the electron hole pair recombination and hence resulting in higher photocatalytic activity. The proximity of the reactant molecules of interest to the electrons and holes is a key factor that contributes to the higher photocatalytic activity. The presence of AC facilitates the adsorption of the molecules of interest and hence they are close enough to the photogenerated electrons and holes and hence to the radicals generated to undergo photodegradation. Moreover, the slight reduction in the band gap of TiO_2/AC compared to pure TiO_2 produces a higher photocatalytic activity. Further, once TiO_2 nanoparticles are added to the reaction mixtures recovery for future use is quite difficult as settling takes a very long time. However, TiO_2 deposited on AC tend to settle quickly and hence the recovery is convenient. However, TiO_2/AC possess some disadvantages as well. Once they are added to the solution the dark colour created, interferes with the absorption of light. Further, AC can cover the TiO_2 surface blocking the light absorption and leading to lower photocatalytic activity. Moreover, the presence of TiO_2 can cover the surface of AC blocking the mesopores and micropores and thus reducing the surface area, decreasing the adsorption capacity.

2.1.2. TiO_2/CNT

2.1.2.1. Degradation of pollutants. Shaban et al. (Shaban et al., 2018) reported the synthesis of TiO_2 nanoribbons (TiO_2 NRs) and carbon nanotube (CNT) composites for the photodegradation of methylene blue under sunlight. It has been observed that the removal of 5 mg/L methylene blue after 240 min via both adsorption and photocatalysis by TiO_2 NRs/CNTs is higher than that of TiO_2 NRs and CNTs individually, due to the enhanced adsorption capacity and increased lifetime of the photogenerated electrons and holes pairs(Zouzelka et al., 2016). TiO_2 NRs removed 12.2 % of methylene blue via adsorption while that by CNTs and TiO_2 NRs/CNTs are 24.6 % and 37.3 %, respectively. The enhanced adsorption by the composite has been attributed to the high surface area and the large number of adsorption sites created due to the growth of CNTs within the pores of TiO_2 NRs. The photocatalytic degradation of methylene blue was 12 % higher in the presence of the composite than TiO_2 NRs while CNTs showed no significant photodegradation. Photocatalytic degradation of dye involves three different stages (1) adsorption of the dye (2) absorption of the light by the catalysts and (3) generation of the required radicals by the charge transfer reactions (Perera et al., 2012). Dyes could be degraded directly by the holes generated during the charge generation or by the hydroxyl radicals generated (Zouzelka et al., 2016)(Akpan & Hameed, 2009). These hydroxyl radicals could be produced by the reaction of holes with the electron donors such as water or hydroxide ions etc. and they could degrade the dye molecules on the surface of the catalyst (Akbal, 2005). As stated above CNTs enhance photocatalytic activity by increasing the lifetime of the charge carriers in addition to adsorbing dyes effectively. The conduction band of TiO_2 is at 4.2 eV while that of CNTs lies at 4.7 eV depending on the number of graphene layers(Yong & Schoonen, 2000). Therefore, the electrons in the CB of TiO_2 are transferred to CNTs and thus the probability of electron hole pair recombination is low (Perera et al., 2012). Electrons are transferred to CNTs until the Fermi level equilibrium is reached, forming a Schottky barrier on the surface. This was demonstrated by the photoluminescence spectra as well where the emission intensity of TiO_2 NRs/CNTs is lower than that of TiO_2 NRs at

Table 1
Synthesis method, textural and optical parameters and the photocatalysis of TiO_2/AC.

Source of AC	Activating method	Coupling method	Surface area of AC (m^2/g)	Surface area of the TiO_2/AC composites (m^2/g)	Band Gap (eV)	Light Source	Pollutant	Concentration of the pollutant (mg/L)	Weight of the catalyst (mg)	Rate constant (min^{-1})/ Conversion	Performance compared to TiO_2	Reference
Lignin	$FeCl_3$ $ZnCl_2$ H_3PO_4 KOH	Solvothermal synthesis	756 1129 807 1446	300 491 435 465	3.28 3.42 3.50 3.45	Suntest solar simulator with a 765–250 Wm^{-2}Xe lamp	Acetaminophen	5	37.5	–	0.73 times 0.40 times 0.60 times 0.51 times	(Manuel Peñas-Garzón et al., 2019)
Lignin	$FeCl_3$	Solvothermal method (ST)	756	300	3.38	Suntest solar simulator with a 765–250 Wm^{-2}Xe lamp	Acetaminophen	5	37.5	ST- 8.3×10^{-3} MW–7.8 $x10^{-3}$ SG – 1.8×10^{-3}	– – –	(M. Peñas-Garzón et al., 2020)
		Microwave-assisted method (MW)		323	3.35		Ibuprofen			ST – 1.8×10^{-2} MW–2.3 $x10^{-2}$	– –	
		Sol-gel route (SG)		130	3.28		Antipyrine			ST – 2.5×10^{-3} MW–4.2 $x10^{-2}$	– –	
Lignin	KOH	Sol-gel route	1576	TiO_2 loading (1), 1507 TiO_2 loading (2), 1167 TiO_2 loading (3), 949	–	450 W high pressure mercury lamp	Rhodamine B	9.6	20	–	1.47 times 1.67 times 1.55 times	(Xing et al., 2016)
Macadamia nut shells	NaOH	Sol-gel route	–	129	3.04	Germicide UV lamp (18 W)	Tetracycline	50	200	42.9×10^{-3}	1.47 times than pure TiO_2 1.22 times than P25	(A. C. Martins et al., 2017)
Purchased from Kermel Chemical Co. ltd.	–	Sol-hydrothermal method	–	–	–	300 W mercury lamp	Cr(VI)	30	250	1.12×10^{-2}	6.23 times	(Fu et al., 2015)
Coconut (Commercial AC S23)	–	So-gel route	1100	962	–	24 W mercury lamp	Tartrazine	320	400	–	–	(Andriantsiferana et al., 2014)
Commercial AC (Darco G-60, Aldrich)	–	Sol-gel route	910	427	–	Low pressure mercury vapor lamp (3 W radiant flux)	Chromotrope 2R*	50	800	8.38×10^{-2}	3.43 times	(W. Wang et al., 2007)
Granular AC	–	Hydrothermal method	1083	985	–	UV lamp (365 nm)	Methyl Orange*	50	500	96.6	–	(Xiaojing Wang et al., 2009)
Powdered AC purchased from Shanghai Zhanyun Chemical Co. ltd	–	Sol-gel route	–	–	–	250 W Xenon UV lamp (365 nm)	2-Methylisoborneol	0.001	3	16.82×10^{-3}	–	(Guo et al., 2021)
AC purchased from Riedel-de-Haën	–	Sol-gel route	767.40	186.36	–	UVA lamps PLS-9 W	Sulfamethazine	15	60	2.5×10^{-2}	–	(Briche et al., 2020)
Commercial AC (Synth, PA)	–	Wet mixing followed by drying	710	165	–	Low-pressure mercury lamp (30 W)	Reactive Black dye	40	60	95	–	(de Oliveira Pereira et al., 2019)

(*continued on next page*)

Table 1 (*continued*)

Source of AC	Activating method	Coupling method	Surface area of AC (m^2/g)	Surface area of the TiO_2/AC composites (m^2/g)	Band Gap (eV)	Light Source	Pollutant	Concentration of the pollutant (mg/L)	Weight of the catalyst (mg)	Rate constant (min^{-1})/ Conversion	Performance compared to TiO_2	Reference
AC purchased from Heng Sheng Huan bao Co. ltd	–	Hydrothermal method	–	–		High pressure mercury lamp (130 W)	Aflatoxin B1	0.001	6	95	–	(de Oliveira Pereira et al., 2019)
Glycerol	H_3PO_3	Sol-gel route	1900.2	1541	2.75	Germicidal UV-C light lamps (15 W) Fluorescent lamps of white light (15 W)	Phenol	50	12.5	UV only ~ 70 % Visible ~ 55 %	1.16 1.43	(Asencios et al., 2022)
Commercial AC (Filtrasorb 400)	–	Sol-gel route	–	–	–	Monochromatic UV lamp, 254 nm (15 W)	Ibuprofen	25	32	92 %	1.53	(Y. Gu et al., 2019)
Argan tree nutshells	H_3PO_4	Impregnation method	1159	959	–	Xenon lamp system (300 W)	Diclofenac Carbamazepine Sulfamethoxazole	50	5	1.931×10^2 0.644×10^2 0.355×10^2	–	(El Mouchtari et al., 2020)

* As there are many catalysts prepared the catalyst with the highest activity was chosen to be included in the table.

the same excitation irradiation intensity. Further, methylene blue molecules absorb photons once exposed to sunlight and excite an electron from the HOMO level to the LUMO level (gap 4.25 eV)(Chatterjee et al., 2017; Z. Zhang et al., 2012). The excited electron at the LUMO level can be lost and the HOMO level requires an electron to achieve the stability. That electron is captured by the water producing hydroxyl radicals which could further degrade methylene blue as shown in Fig. 5. All the reactions involved in the generation of radicals by the composite and photodegradation of methylene blue are given in Eqs. (1) to (8) (Shaban et al., 2018).

$$TiO_2 + hv \rightarrow TiO_2(e^-_{CB}, h^+_{VB}) \quad (1)$$

$$TiO_2(e^-) + CNTs \rightarrow CNTs(e^-) + TiO_2(e^-_{CB}, h^+_{VB}) \quad (2)$$

$$TiO_2(e^-) + O_2 - \rightarrow TiO_2 + O^{\bullet -} \quad (3)$$

$$CNTs(e^-) + O_2 - \rightarrow CNTs + O^{\bullet -} \quad (4)$$

$$TiO_2(h+) + H_2O \rightarrow TiO_2 + H+ + OH^{\bullet} \quad (5)$$

$$(TiO_2)e + MB \rightarrow (TiO_2)e^- + MB^{+\bullet} \quad (6)$$

$$MB^{+\bullet} + O_2^- \rightarrow Degradedproducts \quad (7)$$

$$MB^{+\bullet} + OH^{\bullet} \rightarrow Degradedproducts \quad (8)$$

Huang et al. (Y. Huang et al., 2018) reported the enhanced photocatalytic activity of TiO_2/CNT/reduced graphene oxide composite synthesized by solvothermal method, for the photodegradation of Rhodamine B under UV-visible irradiation generated by a 300 W Xenon lamp. As shown in the TEM image (Fig. 6(a)) TiO_2 nanoparticles are not only dispersed on reduced graphene oxide but also, are absorbed into CNTs. Further, it could be seen that CNT is intercalated into reduced graphene oxide (rGO) sheets which improves the speed of electron migration and hence the photocatalytic activity(Fan et al., 2010). Graphene oxide and oxide-treated CNTs were combined via π-π interactions formed during the ultrasonication. rGO proportion was kept constant while the quality ratio of TiO_2:CNT was varied as 0.5, 1, 2, 3, 5 and 10 %. The photocatalytic activity increased with an increasing proportion of CNT up to 3 % and decreased with further increments. TiO_2/CNT/rGO −3% showed higher photocatalytic activity than TiO_2/CNT, TiO_2/rGO, and pure TiO_2 as shown in Fig. 6(b and c). The high performance of TiO_2/CNT/rGO has been attributed to the presence of rGO and CNT as they possess a large surface area and the high number of adsorption sites

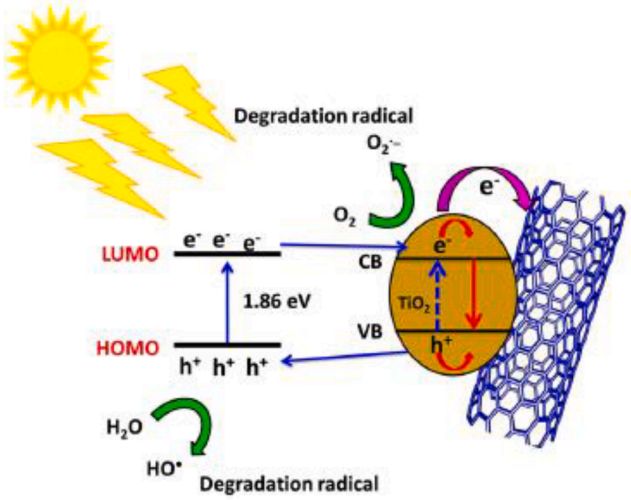

Fig. 5. Scheme illustrating the mechanism of photodegradation of methylene blue by TiO_2 NRs/CNTs. Figure adapted from. ref. (Shaban et al., 2018). (For interpretation of the references to colour in this figure legend, the reader is referred to the web version of this article.)

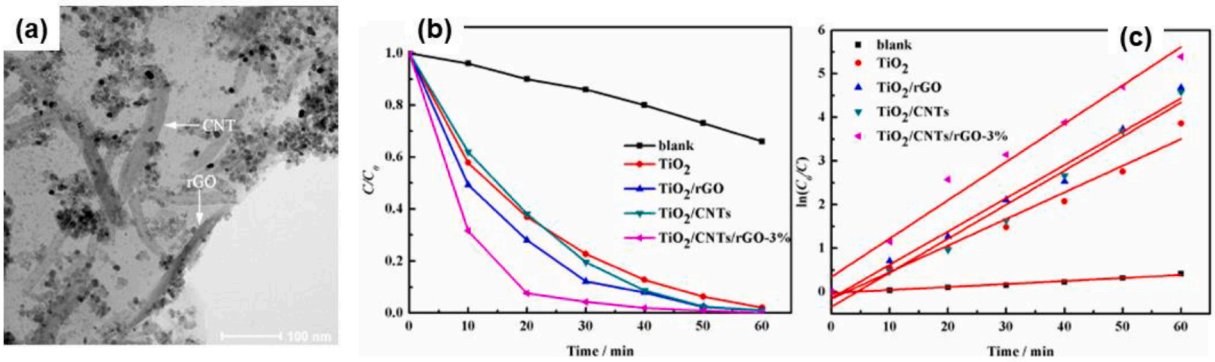

Fig. 6. (a) TEM image showing the dispersion of Nanoparticles with respect to rGO and CNTs (b) C/C0 vs time (c) first order kinetics plot. Figure adapted from Figure (Y. Huang et al., 2018).

to O_2, H_2O and organics facilitating the production of $OH^{\bullet}$ which eventually degrade dye molecules (Y. Huang et al., 2018). Further, the oxidation-reduction ability is increased, and the rate of electron hole pair recombination is reduced by the incorporation of CNTs (Sampaio et al., 2018). Moreover, CNTs prevent the stacking of rGO and enrich the active sites for photocatalytic reaction(Lv et al., 2014). When the composites are exposed to UV-Visible light, photogenerated electrons and holes are produced at TiO_2 (Eq. (9)) while the Rhodamine B, dye molecules also absorb the photon flux (Eq. (10))(Rastogi et al., 2016). Reduced graphene oxide and CNT capture the photogenerated electrons and transfer them to the dye molecules increasing the number of participating electrons (Eqs. (11) and (12))(Rastogi et al., 2016). Reduced graphene oxide and CNT serve as adsorption sites to O_2, H_2O and organics due to the high surface area and these species further form H_2O_2 (Eqs. (13) and (14))(Sampaio et al., 2018). H_2O_2 capture the electrons and form OH^- and $OH^{\bullet}$ while the holes react with OH^- and H_2O to produce $OH^{\bullet}$ (Eq. (15) to (19)) (C. Wang et al., 2014). The radicals formed, $O_2^{-\bullet}$ and $OH^{\bullet}$ degraded Rhodamine B molecules to colorless products.

$$TiO_2 + h\upsilon \rightarrow TiO_2(h^+ + e^-) \quad (9)$$

$$RhB + h\upsilon \rightarrow RhB^*(h^+ + e^-) \quad (10)$$

$$rGO + e^- \rightarrow rGO(e^-) \quad (11)$$

$$CNTs + e^- \rightarrow CNTs(e^-) \quad (12)$$

$$rGO(e^-) + O_2 + 2H^+ \rightarrow rGO + H_2O_2 \quad (13)$$

$$H_2O_2 + h\nu \rightarrow 2OH^- \quad (14)$$

$$H_2O_2 + e^- \rightarrow OH^- + OH^{\bullet} \quad (15)$$

$$OH^- + h^+ \rightarrow OH^{\bullet} \quad (16)$$

$$CNTs(e^-) + O_2 \rightarrow CNTs + O_2^{-\bullet} \quad (17)$$

$$TiO_2(h^+) + OH^- \rightarrow TiO_2 + OH^{\bullet} \quad (18)$$

$$TiO_2(h^+) + H_2O \rightarrow TiO_2 + OH^{\bullet} \quad (19)$$

Awfa et al. (Awfa et al., 2019)reported the adsorption and photocatalytic activity of magnetic CNT-TiO_2 (MCNT-TiO_2) on pharmaceuticals, carbamazepine and sulfamethoxazole. MCNT-TiO_2 showed adsorption equilibrium in the range of 1–1.4 mg/g, which was greater than that of pure TiO_2 (0.2 mg/g). Molecules adsorb to TiO_2 electrostatically and via ligand exchange (K. Yang & Xing, 2009). The presence of CNT in MCNT-TiO_2 enhances the adsorption via hydrophobic interaction, hydrogen bonds, and electrostatic interactions (Ateia et al., 2017). Carbamazepine as a neutral molecule adsorbs through hydrophobic and π-π interactions (Maeng et al., 2015). Sulfamethoxazole of which the pKa_1 and pKa_2 are 1.85 and 5.6, respectively, adsorb via electrostatic interactions as sulfamethoxazole appears to be anionic in neutral pH (Hanyu Zhang et al., 2017). Self-photolysis of carbamazepine is negligible under solar energy as functional groups that absorb light of >290 nm are absent (Y. Wang et al., 2017). However, 20–50 % of sulfamethoxazole degrades due to the presence of phenylamine functional groups which absorbs >290 nm (Boreen et al., 2004). The highest rate constant (6.8×10^{-2} min^{-1}) for degradation of carbamazepine was obtained in the presence of MCNT-TiO_2 and that is 1.5 times greater than that of pure TiO_2 (4.6×10^{-2} min^{-1}). The maximum synergistic effect and hence the maximum photocatalytic activity is obtained when MCNT and TiO_2 are mixed with a ratio of 1:5. Photocatalytic activity is enhanced in the presence of CNTs due to (1) transfer of excited electrons of MCNT to TiO_2 (2) excited electrons of MCNTs react with molecular O_2 to produce superoxide radicals (3) MCNT provides adsorption cites acting as an electron sink and improve the visible light absorption as the band gap reduced due to the presence of Ti—O—C bond. However, the photocatalytic activity decreased once the content of MCNT further increased due to the aggregation of TiO_2 on MCNT which reduces the number of active sites and photocatalysis (Song et al., 2012). Moreover, MCNT screen the light and prevent the photocatalytic reaction (F. Wang & Zhang, 2011). The photocatalytic activity of degrading the pharmaceuticals is reduced in all the tested photocatalysts with the natural organic matter (NOM) in the medium due to the competitive adsorption of NOMs to the catalyst surface limiting the carbamazepine and sulfamethoxazole adsorption. However, the reduction of the photocatalytic activity was less with MCNT-TiO_2 compared to the others because despite the competition MCNT provides active sites due to the high surface area. Further, NOMs limit the photocatalytic activity as they act as scavengers of hydroxyl radicals ($OH^{\bullet}$), superoxide and holes generated and thus reduce the photodegradation of the pharmaceuticals (Awfa et al., 2019).

Hydrothermally synthesized multiwall carbon nanotube/TiO_2 nanotube (MWCNT/TNT) composites have shown excellent photocatalytic activity in degrading RhB under UV light (Natarajan et al., 2017). A schematic illustration of the synthesis procedure is given in Fig. 7(a). Composites have been synthesized varying the loading of MWCNT as 1, 3, 5, 7 and 10 % and the highest photocatalytic activity was obtained with 10 % of MWCNT. The distribution of TNT and MWCNT is shown in the TEM image (Fig. 7(b)) and the HRTEM image (Fig. 7(c)) exhibits the intimately bound MWCNT to TNT. Drastic decrease in the intensity of photoluminescence spectra shown in Fig. 7 (d) reveals that the electron hole pair recombination is minimum in 10 % MWCNT/TNT compared to the MWCNT, anatase nanoparticles (AT) and TNT reasoning for the resulted highest photocatalytic activity of 10 % MWCNT/TNT. Being consistent with the above-described research works described in section 2.1.2 CNTs trap the photogenerated electrons produced by TiO_2 effectively separating the holes and electrons and thus minimizing the electron hole pair recombination. Electrons once transferred to the surface CNT react with adsorbed and dissolved oxygen and

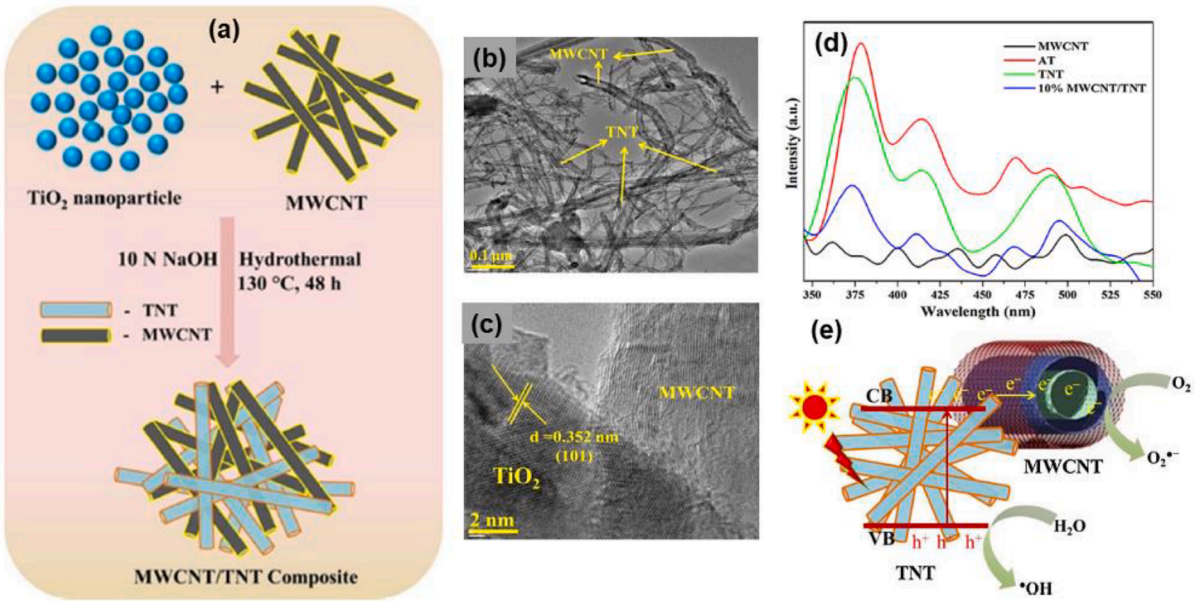

Fig. 7. (a) schematic illustration of the synthesis procedure (b) TEM (c) HRTEM image of 5%MWCNT/TNT (d) PL spectra of MWCNT, AT, TNT and 10%MWCNT/TNT (e) schematic representation of the mechanism of electron hole separation and radical formation. Adapted from ref. (Natarajan et al., 2017).

produce superoxide radicals ($O_2^{\bullet-}$) while holes react with H_2O and OH^- in the medium producing hydroxyl radicals ($OH^{\bullet}$) which effectively degrade RhB dye molecules as illustrated in Fig. 7(e). Degradation of RhB was further supported by the %COD and %TOC values where they increased with increasing loading of MWCNT reaching the maxima of 83 % and 64 %, respectively, when 10 % MWCNT/TNT was used as the photocatalyst (Natarajan et al., 2017).

Sharma et al. (H. K. Sharma et al. (2021b))reported the synthesis of TiO_2/CNT composite by a hydrothermal method where the morphology of TiO_2 was nanoflowers, and the use of the synthesized photocatalysts to degrade methylene blue under irradiation produced by a solar simulator. The surface area of CNT (166.53 m^2/g) was reduced to 49.96 m^2/g when coupled with TiO_2 because the TiO_2 nanoparticles enter into the pores of CNT and decrease the surface energy due to the agglomerated TiO_2 nanoparticles. The band gap of TiO_2 (3.0 eV) was reduced to 2.7 eV by coupling with CNTs. The rate of photodegradation of methylene blue in the presence of TiO_2/CNT (0.01467 min^{-1}) is higher than that of TiO_2 (0.01343 min^{-1}) and CNT (0.00515 min^{-1}) due to the formation of new electronic inter bands or donor levels below the conduction band with the formation of Ti-C and Ti—O—C bonds (H. K. Sharma et al. (2021b)). Wang et al. (L. Wang et al., 2018a) reported the synthesis of TiO_2/AC and TiO_2/CNT and their photocatalytic activity on the degradation of methyl orange under UV irradiation. AC sieved through 70, 100, 160 and 200 meshes were treated with HCl followed by calcination and they were coupled with TiO_2 via sol-gel synthesis method followed by calcination in N_2 atmosphere at 823 K. CNT functionalized with concentrated HNO_3 was coupled with TiO_2 in the same way where TiO_2/CNT was supported on a glass slide. Further, TiO_2 doped with Bi, Mn, Zn and Ni were also coupled with AC and CNT to study the effect of doping on photocatalysis. TiO_2 coupled to AC sieved at 160 showed the highest photocatalytic activity. Externally added anions, Cl^-, SO_4^{2-} and NO_3^- promoted the photocatalytic activity due to the production of $OH^{\bullet}$ which degrades the methyl orange molecules while 3 % H_2O_2 significantly enhances the photocatalytic reaction by inhibiting the electron hole pair recombination and by providing $OH^{\bullet}$ to the medium. The photocatalytic activity was also increased by co-doping TiO_2 with Bi-Ni-Mn and Bi-Mn-Zn due to the excellent charge carrier separation and migration of them to the diverse active sites at the semiconductor/liquid interface. Overall activity of TiO_2/CNT supported on glass slide was lower than that of TiO_2 coupled to AC sieved at 160. Though CNT has many functional groups which methyl orange could adsorb easily under narrow UV light with high energy functional groups were destructed limiting the adsorption of methyl orange. Under UV light irradiation composite detached from the glass slide further, decreasing the photocatalytic activity (L. Wang et al., 2018a).

TiO_2/CNT composites have been further reported to be effective in degrading 4-chlorophenol(Zouzelka et al., 2016), nitrobenzene (Ling et al., 2016), iopamidol, iopromide, diatrizoic acid, diclofenac, triclosan and sulfamethoxazole (Murgolo et al., 2015), eosin yellow (Kuvarega & Mamba, 2016), Bismarck brown R dye(Kamil et al., 2018) while Graphene-CNT-TiO_2 composites have been reported to be effective in the removal of MB and Cr (VI) (C. Wang et al., 2014) etc. Table 2 summarizes the synthesis method and the photocatalysis of TiO_2/CNT reported in the literature.

2.1.2.2. Advantages and disadvantages. The main advantage of coupling the TiO_2 nanomaterials with CNT is the enhancement of the photocatalysis due to the improved adsorption of the pollutants, increased charge separation minimizing the electron hole pair recombination, efficient charge transfer to interested species like H_2O and O_2 to produce the radicals which are responsible in degrading the pollutants. Further, CNT prevents the TiO_2 nanoparticle aggregation by providing sufficient sites to adhere to the TiO_2 nanoparticles. Hence, the dispersion of the nanoparticles leads to higher photocatalytic activity. The main drawback associated with CNT is the blocking of the irradiation, UV, visible light or sunlight at higher CNT loading limiting the photons reaching the photocatalysts and hence reducing the production of the radicals lowering the photocatalytic activity. Additionally, the preparation of CNT requires sophisticated methods like CVD which are not available throughout the world, especially in developing countries and handling and maintaining such instruments are expensive. Moreover, the carbon precursors used for the preparation of CNT such as C_2H_2 and the method of introduction of such material; the flux of the precursor in a tube furnace at elevated temperatures also contribute to the high production cost.

Further, the presence of other elements like Fe, Co and Al in trace amounts in the final fabricated photocatalysts which were added as the catalysts during the preparation of CNT also contribute to the activity which interferes with the conclusions in photodegrading the pollutants.

Table 2
Synthesis and photocatalytic performance of TiO_2/CNT selected from the literature.

Morphology of TiO_2	Coupling method	Surface area (m^2/g)	Band Gap (eV)	Light source	Pollutant	Concentration of the pollutant (mg/L)	Weight of the catalyst (mg)	Rate (min^{-1})/ conversion	Performance compared to TiO_2	Reference
Nanoribbon	Hydrothermal	102.75	3.09	Sun light	Methylene blue	5	20	2.81×10^{-2}	2.5 times	(Shaban et al., 2018)
Nanoparticle	Solvothermal	–	–	300 W Xenon lamp	Rhodamine B	10	10	8.785×10^{-2}	1.5 times	(Y. Huang et al., 2018)
Nanoparticle	Sonication followed by drying	151	–	A solar simulator at an intensity of 1000 W m^{-2}	Carbamazepine	0.15	20	6.8×10^{-2}	1.4 times	(Awfa et al., 2019)
Nanotube	Hydrothermal	275	3.11	125 W mercury vapour lamp	Rhodamine B	50	50	89 %	1.6 times	(Natarajan et al., 2017)
Nanoparticle	Sonication followed by drying	101 m^2/cm^3	~ 2.8	11 W BLB lamp	4-Chlorophenol	13	–	4.2×10^{-3}	1.9 times	(Zouzelka et al., 2016)
Nanoparticle	Hydration and evaporation-drying process	–	–	6-W black-light blue lamps	Nitrobenzene	0.6	1.2	1.18×10^{-2}	2.46 times	(Ling et al., 2016)
Clusters	Sonication followed by calcination	–	3.15	500 W Xenon lamp	Eosin yellow	100	100	3.220×10^{-2}	8 times	(Kuvarega & Mamba, 2016)
Nanoparticle	Sol–gel method, and simple evaporation and drying	–	2.8	UV lamp (0.7 mW/cm^2)	Bismarck brown R dye	23	50	1.32×10^{-2}	2.28 times	(Kamil et al., 2017)
Nanoparticle	Sonication followed by calcination	59.9	–	4 W UV-filtered lamp	Methylene Blue	10	0.04	~90	~1.12 times	(Park et al., 2018)
Nanoparticle	Sol–gel method and calcination	–	1.93	300 W Xe lamp	Methylene Blue Rhodamine B Congo Red Methyl Orange Phenol	100	50	0.15 0.0452 0.0808 0.0147 0.0412	–	(Akter, Hanif, Islam, Sapkota, & Hahn, 2021)
Nanoparticle	Sonication followed by drying	84.75	–	60 W UV lamp	Phenol	10 20 30	300	98.74 96.46 74.32	1.08 times – –	(Vaziri et al., 2021)
Nanoflower	Hydrothermal	49.96	2.7	Solar simulator	Methylene Blue	5	100	1.467×10^{-2}	1.09 times	(H. K. Sharma et al., 2021)
Nanoparticle	Supercritical synthesis followed by calcination	156	2.34	70 W Visible light LED lamp	Dibutylhydroxytoluene	0.5	70	7.0×10^{-3}	1.4 times	de la Flor et al. (2021)

2.1.3. TiO_2/Graphene derivatives

2.1.3.1. Degradation of pollutants. TiO_2/graphene nanocomposites synthesized as a one-pot synthesis via the chemical exfoliation method have been effective in degrading MB using visible light generated by a 300 W xenon short-arc lamp and a 422-nm long-pass filter (Ton et al., 2018). Graphene dispersions were prepared in both titanium tetra *n*-butoxide (Ti(O*n*Bu)$_4$) and benzylamine which is the most frequently used exfoliating solvent. Nanocomposites were synthesized by a simple sol-gel synthesis method where either H_2O or NH_3 dissolved in benzylamine was added dropwise to the graphene-Ti(O*n*Bu)$_4$ dispersion to catalyze the hydrolysis of the titanium precursor and form TiO_2. TiO_2/reduced graphene oxide(rGO) composites were also prepared by the method reported by Jiang et al (B. Jiang et al., 2011). According to the Raman spectroscopic analysis and atomic microscopic analysis it has been found that the quality of graphene prepared in Ti(O*n*Bu)$_4$ was superior to that produced in benzylamine. As shown in the Raman spectra (Fig. 8(a)). The FWHM of the 2D band (28 cm^{-1}) of graphene synthesized in Ti(O*n*Bu)$_4$ suggests the presence of few graphene layers compared to the graphene layers produced in graphene prepared in benzylamine as indicated by the broadened 2D peak with the FWHM of 70 cm^{-1}. AFM images exhibited in Fig. 8(b and c) of graphene produced in Ti(O*n*Bu)$_4$ and benzylamine, respectively, reveal that the thickness of the graphene layers of graphene produced in Ti(O*n*Bu)$_4$ is 2 nm while that in graphene produced in benzylamine is 4 nm being consistent with the Raman analysis. The adsorption of MB by the graphene-containing photocatalysts was higher than that of P25 due to the high surface area and the greater affinity of the MB molecules to graphene. The latter is resulted due to the physisorption and but also via chemisorption resulted because of π-π interactions occur between the aromatic rings of MB and aromatic domains of graphene layers (F. Liu et al., 2012). Photocatalysis of TiO_2/graphene (catalyzed by NH_3 in benzylamine) is 5 times higher than that of TiO_2/rGO and 15 times higher than that of P25 TiO_2 (Fig. 8(d)). This is due to the special morphology where graphene

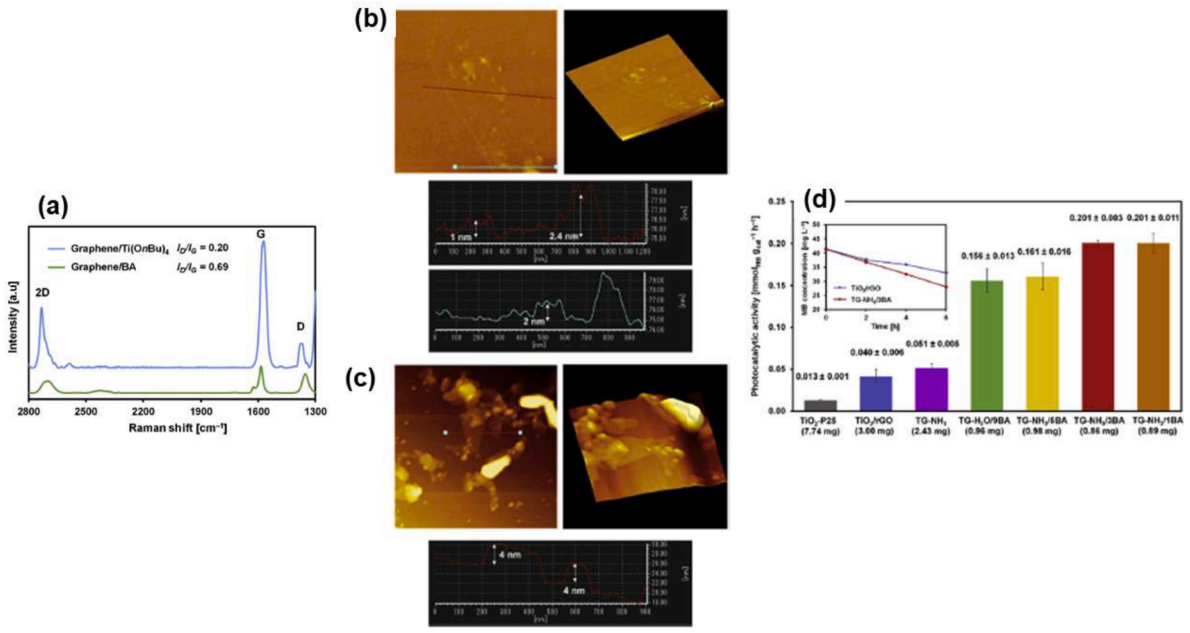

Fig. 8. (a) Raman spectra of graphene prepared in Ti(O*n*Bu)$_4$ and Benzylamine, AFM images and line profiles of (b) graphene prepared in Ti(O*n*Bu)$_4$ (c) graphene prepared in Benzylamine (d) photocatalytic activity of the synthesized catalysts, insert – a variation of MB concentration with time. Figure adapted from. ref. (Ton et al., 2018).

layers are covered by TiO_2 led to the higher adsorption of MB, and extended absorption edge which enhanced the visible light absorption and the charge separation resulting due to the thin TiO_2 layer covering graphene sheets and the low defect density of graphene (Ton et al., 2018). Similarly, Liu et al. (X. Liu et al., 2018) also reported enhanced adsorption of MB to TiO_2 baring graphene oxide which has been attributed to the same fact of forming π-π interactions. Interestingly, as they studied the effect of the morphology of the TiO_2 nanomaterial for the adsorption and then the photodegradation of MB, they observed enhanced adsorption of MB to TiO_2 spheres. TiO_2 spheres and rods had different contents of major exposed crystalline planes. TiO_2 spheres mainly expose the {001} faces while the density of broken bonds {001} faces were greater than that on {101} and {100} faces. TiO_2 nanorods possess {001} and {101} faces as the major exposed crystalline faces. Hence, the density of broken bonds in TiO_2 sphere-graphene composite is higher than in TiO_2 nanorods-graphene composite leading to a higher adsorption capacity (S. Liu et al., 2010). Further, the abundancy of Ti—O—C bonds in between TiO_2 and graphene is high in TiO_2 sphere-graphene composite than that of TiO_2 nanorods-graphene composite leading to a larger decrement in the band gap resulting in higher photocatalytic activity (X. Liu et al., 2018).

TiO_2/graphene oxide (GO) composites have shown remarkable photocatalytic activity in the degradation of MB and ciprofloxacin under sunlight. TiO_2 was synthesized using Diammonium hexaflourotitanate as the titanium precursor and GO was synthesized by adopting the Hummer's and Hoffman's method (Khan et al., 2019). TiO_2 was deposited on graphene oxide nanosheets by liquid phase deposition. GO was introduced varying the amount of GO as 2, 4, 6, and 8 %. TiO_2/GO (8 %) showed the highest photocatalytic activity on degrading MB and ciprofloxacin. TiO_2/GO (8 %) degraded 98.67 % of MB after 45 min, while in the presence of pure TiO_2 could degrade only 52.0 % even after 120 min. A similar trend was observed with the photodegradation of ciprofloxacin where 96.73 % was degraded in the presence of TiO_2/GO (8 %), while only 65.52 % was degraded in the presence of pure TiO_2. Further, the photocatalytic activity increased with the increasing amount of GO. MB and ciprofloxacin are positively charged and the COOH groups present on GO render an electron-rich or a negative charge facilitating the electrostatic interactions between the molecules of interest and the GO surface. Further, π-π interactions are also formed especially between the aromatic MB and aromatic regions of GO as illustrated in Fig. 9. These interactions enhance the concentration of MB and ciprofloxacin close to the catalyst surface and ultimately enhances the photocatalytic activity. Further, GO enhance the separation of electron hole pairs as they capture the electrons and transfer them to O_2 to form superoxide radicals. Additionally, high surface area (91.25 m^2/g), smaller pre volume (0.12 cm^3/g), low band gap (2.47 eV) and the more crystalline nature of TiO_2/GO (8 %) contributed to the resulted in higher photocatalytic activity. Moreover, the authors have found that the photocatalytic activity decreased with the introduction of EDTA-2Na, *tert*-butanol, *p*-benzoquinone and N_2 gas because EDTA-2Na scavenges holes, *tert*-butanol, *p*-benzoquinone scavenge hydroxyl radicals and superoxide radicals while the concentration of dissolved O_2 is decreased by bubbling N_2 gas. Hence, those were the active species in degrading MB and ciprofloxacin (Khan et al., 2019).

Martins et al. also observed a similar trend in degrading MB and ciprofloxacin under UV, in the presence of TiO_2/graphene and TiO_2/graphene oxide (P. M. Martins et al., 2018). Comparatively higher rate constants for the degradation of MB were obtained in the presence of composites with the highest incorporation of graphene and GO, TiO_2/graphene(3 %) (0.160 min^{-1}) and TiO_2/graphene oxide (1.5 %) (0.115 min^{-1}), respectively. Similarly, higher degradation of ciprofloxacin was obtained with the same photocatalysts, 0.016 min^{-1} and 0.014 min^{-1}(P. M. Martins et al., 2018). Further, Zhang et al. reported the superior photocatalytic activity on photodegradation of MB in the presence of P25-graphene oxide (85 %) compared to P25-CNT (70 %) and P25 (12 %) (Hao Zhang et al., 2010). Raja et al. reported that 96.2 % of ciprofloxacin could be photodegraded in the presence of hydrothermally synthesized TiO_2/rGO, while only 79.7 % was degraded by P25 under visible light generated by a tungsten lamp (150 mW/cm^{-2}) (Raja et al., 2019).

Adly et al. (Adly et al., 2019) reported that the hydrothermally synthesized TiO_2/graphene oxide is capable of photodegrading RhB and acid green 25 dyes under UV-Visible light generated by a Hg lamp. GO was incorporated as 3, 7, 10, 12, and 15 % relative to TiO_2. It was observed that TiO_2/GO (10 %) showed the highest photocatalytic activity. The rate constant for the photodegradation of RhB in the presence

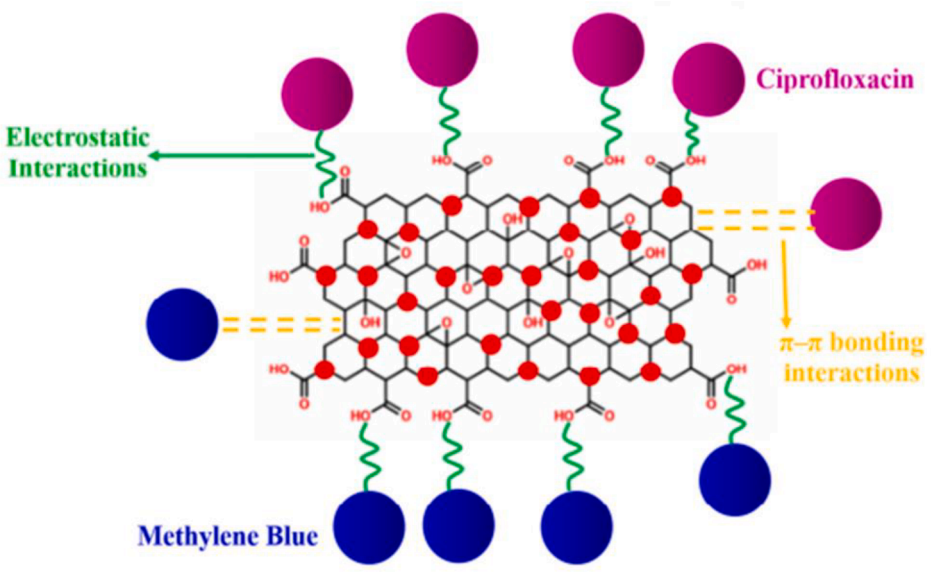

Fig. 9. The adsorption behaviour of MB and ciprofloxacin by TiO_2/GO (8%). Figure adapted from. ref. (Khan et al., 2019).

of TiO_2/GO (10 %) was 0.051 min^{-1} and that for the degradation of acid green 25 was 1.577×10^{-6} min^{-1}. The rate constant for the degradation of the same dyes by pure TiO_2 were 0.033 and 0.948×10^{-6} min^{-1}, respectively. Therefore, it is evident that the photocatalytic activity for the degradation of RhB and acid green 25 dye in the presence of TiO_2/GO (10 %) is 1.5 and 1.7 times, respectively, greater than pure TiO_2. Though the photocatalytic activity increased with the increasing amount of GO up to 10 %, it decreased with further increments of GO content due to the increasing light absorption into the GO sheets and relative lower content of TiO_2 in a given mass which then leads to the production of a lower number of radicals (Table 3) (Adly et al., 2019).

Niazi et al. (Niazi et al., 2021) reported the synthesis of TiO_2 coupled to graphene quantum dots and their photocatalytic activity on degradation of Reactive Black 5, the textile dye under sunlight. Graphene quantum dots were prepared by pyrolysis of citric acid (Dong et al., 2012; Roushani et al., 2015) and coupled with hydrothermally synthesized TiO_2 nanoparticles via the solvothermal method. The specific surface areas of TiO_2 nanoparticles and TiO_2/Graphene quantum dots were 235.87 and 133.32 m^2/g, respectively. The band gap of Graphene quantum dots, TiO_2, and TiO_2/Graphene quantum dots are 4.40, 2.23 and 2.13 eV, respectively. Composite has shown photocatalytic activity on degrading Reactive Black 5 under sunlight. The conversion of the dye to harmless species increased from 63.0 % to 100.0 % with increasing catalyst loading 0.2–0.8 g/L and decreased with further increment to 1.0 g/L due to aggregated nanoparticles which led to a reduction in the surface area. The photocatalytic activity was not reduced upon the addition of methanol and isopropanol which are hole and OH_{bulk} scavengers, respectively. However, the rate decreased when NaF and benzoquinone, which are $OH^{\bullet}$ and $O_2^{-\bullet}$ scavengers, respectively, are added indicating the reactive species that are responsible for the dye degradation are $OH^{\bullet}$ and $O_2^{-\bullet}$(Niazi et al., 2021). TiO_2/graphene derivatives have shown remarkable photocatalytic activity for the degradation of RhB (M. H. H. Ali et al., 2018; Gunnagol & Rabinal, 2018; Hardiansyah et al., 2021), methylene blue (Minella et al., 2017; Najafi et al., 2017; Rong et al., 2015), 2,4-dichlorophenoxyacetic (Natarajan et al., 2021), NO_x (Trapalis et al., 2016) etc. Table 4 summarizes the synthesis method and the photocatalysis of TiO_2/graphene derivatives reported in the literature.

Table 3
Rate constants and R^2 values for the photodegradation of RhB and Acid green 25 using TiO_2/GO catalysts calcined at 400 °C. Reproduced from ref. (Adly et al., 2019).

Sample	RhB		Acid green 25	
	k (min^{-1})	R^2	k (min^{-1})	R^2
Pure TiO_2	0.033	0.942	0.948×10^{-6}	0.983
3 wt% GO/TiO_2	0.037	0.978	0.558×10^{-6}	0.942
7 wt% GO/TiO_2	0.034	0.981	0.759×10^{-6}	0.974
10 wt% GO/TiO_2	0.051	0.984	1.577×10^{-6}	0.984
12 wt% GO/TiO_2	0.041	0.948	0.781×10^{-6}	0.944
15 wt% GO/TiO_2	0.036	0.985	0.732×10^{-6}	0.948

2.1.3.2. Advantages and disadvantages. Coupling TiO_2 with graphene derivatives including graphene, graphene oxide and reduced graphene oxide possesses advantages such as improved adsorption of the pollutants due to the functional groups present such as COOH, especially in graphene oxide. Further, the interconnected porosity and the high surface area of the graphene derivatives enhance the adsorption of pollutants. The proximity of the pollutants to the catalyst surface and hence to the produced radicals lead to higher photocatalytic activity. Further, highly conductive graphene derivatives capture the photogenerated electrons and facilitate the transfer the charges to produce radicals. The main disadvantage of graphene derivatives is that they mask the photocatalysts when coupled at higher percentages and reduce the light penetration which lowers the production of radicals and hence decreases the photocatalysis. The dark opaque colour generated by the black colour graphene derivatives further interferes with the UV-Visible spectroscopic measurements. Some of the harsh conditions supplied in the synthesis of graphene oxide such as the use of concentrated acids and the resultant exothermic reaction conditions make the synthesis difficult.

2.2. Visible active TiO_2/Carbon-based materials

2.2.1. TiO_2/g-C_3N_4

2.2.1.1. Degradation of pollutants. Graphitic carbon nitride (g-C_3N_4) has attracted tremendous interest in the last few decades due to its many promising electric, optical and physicochemical properties (Wen et al., 2017; Jian Xu et al., 2015; Jingsan Xu et al., 2014). It is a metal-free nanoplatform that was first reported for its photocatalytic activity in 2009 when it was used for water splitting to produce H_2 and O_2 using solar energy by Wang et al (Xinchen Wang et al., 2008). Different allotropes of C_3N_4 including a-C_3N_4, b-C_3N_4, graphitic-C_3N_4, cubic-C_3N_4,

Table 4
Synthesis and photocatalytic performance of TiO_2/Graphene derivatives selected from literature.

Graphene derivative	Coupling method	Surface area (m^2/g)	Band gap (eV)	Light source	Pollutant	Concentration of the pollutant (mg/L)	Weight of the Catalyst (mg)	Rate (min^{-1})/ Conversion	Performance compared to TiO_2	Reference
Graphene	Sol-gel synthesis	–	3.39 2.33	300 W xenon short arc lamp and a 422-nm longpass filter	Methylene blue	50	89	0.201 mmol $gcat^{-1}h^{-1}$ *	15 times	(Ton et al., 2018)
Graphene oxide	Solvothermal method	94.548	3.13	UV lamp (30 W)	Methylene blue	50	50	8.70×10^{-3}	1.4 times	(X. Liu et al., 2018)
Graphene oxide	Liquid phase deposition	91.25	2.47	Sun light	Methylene blue Ciprofloxacin	5	50	98.67 % 96.73 %	1.9 times 1.5 times	(Khan et al., 2019)
Graphene	Hydrothermal method	–	2.75	UV source 8 W mercurial fluorescent lamps with a flux of 1.6–1.7 mW/cm^2	Methylene blue Ciprofloxacin	0.5	50	1.60×10^{-1} 1.6×10^{-2}	2.3 times The activity of TiO_2 is 1.37 times greater	(P. M. Martins et al., 2018)
Graphene oxide		–	2.53	Visible source Ingenieurburo Mencke & Tegtmeyer GmbH sun simulator, with a flux of 9.8 mW/cm^2	Methylene blue Ciprofloxacin			1.15×10^{-1} 1.4×10^{-2}	1.6 times The activity of TiO_2 is 1.57 times greater	
Graphene oxide	Hydrothermal method	51.034	2.88	100 W high pressure Hg lamp	Methylene blue	10	30	85 %	7 times	(Hao Zhang et al., 2010)
Reduced graphene oxide	Hydrothermal method	–	2.7	Tungsten lamp (150 mW/cm^2)	Ciprofloxacin	13.25	30	96.2 %	1.2 times	(Raja et al., 2019)
Graphene oxide	Hydrothermal method	–	2.98	Hg lamp	Rhodamine B Acid green 25	10 40	50	5.1×10^{-2} 1.577×10^{-6}	1.5 times 1.7 times	(Adly et al., 2019)
Reduced graphene oxide	Microwave irradiation followed by drying	–	3.22	UV irradiation ($\lambda = 352$ nm)	Rhodamine 6G	10	10	82.9 %	2.7 times	(Hardiansyah et al., 2021)
Graphene oxide	Solvothermal method	80.56	3.43	Medium pressure Mercury lamp, 125 W with the presence of UV-light	2,4-dichlorophenoxy acetic acid	50	25	86.4 %	1.4 times	(Natarajan et al., 2021)
Graphene oxide	Solvothermal method	138.01	3.16	UV source UV-A light source (15 W) Irradiation level at the sample ~10 W/m^2	NO_x	50	–	42.86 %	1.7 times	(Trapalis et al., 2016)
				Visible source 8 W 4000 K lamps Irradiation level at the sample ~7000 lx				22.34 %	2.4 times	
Graphene quantum dots	Solvothermal method	133.32	2.13	Sunlight	Reactive Black 5	50	48	1.6×10^{-1}	–	(Niazi et al., 2021)

* Unit was not unified as sufficient data was not available.

and pseudo-cubic-C_3N_4 are reported and among them, graphitic-C_3N_4 is most stable under ambient conditions (G. Liao et al., 2019; Xinchen Wang et al., 2008). It could be produced by different starting materials such as urea, thiourea, melamine, cyanamide etc (Reddy et al., 2019). It is comprised of s-triazine or tri-s-triazine units as the monomers, which form honeycomb-like two-dimensional (2D) sheets via interconnecting the building blocks through ternary amines. These 2D sheets are held together via Van der Waals forces and the atoms of one sheet are covalently bound to each other (Ong et al., 2016). g-C_3N_4 is well known for its remarkable photocatalytic activity resulting in due to the sensible absorption of sunlight, efficient charge carrier separation, high surface area etc, (Wen et al., 2017). The valence band of g-C_3N_4 consists of N 2p level only, while the conduction band is formed by the hybridization of N 2p and C 2p levels. Therefore, the photogenerated electrons are available in the N 2p and C 2p levels and the photogenerated holes present in N 2p level led to charge carrier recombination, which eventually leads to low photocatalytic efficiency. In order to minimize the electron hole pair recombination, many strategies have been implemented including doping with other elements, incorporation of co-catalysts and formation of heterostructures (Chen et al., 2018; Zeng et al., 2019). Among them, the latter has been researched more as a maximum charge separation could be achieved due to the delocalized conjugated π structure (J. Zhang et al., 2011) and the negative potential (−1.12 eV vs NHE) of the lowest unoccupied molecular orbital (H. Wei et al., 2017b). g-C_3N_4 couple to metal oxides exhibits improved photocatalytic performance due to the enhanced charge separation. Band alignments of the two semiconductors can lead to two different conformations as type II and Z-scheme heterojunctions. The two semiconductors used to describe the heterojunctions will be denoted as semiconductors A and B. The position of the VB of semiconductor A is higher than that of semiconductor B in type II heterojunctions. Due to the differences in voltages, photogenerated holes at the VB of semiconductor B migrate to the VB of semiconductor A, and the electrons at the CB of semiconductor A to that of semiconductor B as shown in Fig. 10(a). The separation of photoinduced electrons and holes leads to low electron hole pair recombination and increases the lifetime of electrons leading to an enhanced photocatalytic activity. On the other hand, in Z-scheme heterojunctions (Fig. 10(b)) the photogenerated electrons on the CB of semiconductor B transfer to the VB of semiconductor A. This not only leads to charge separation reducing electron hole pair recombination but also improves the redox ability (Ren et al., 2019). Though there is a chance of recombining electrons and holes producing photons, other photogenerated charge carriers replace them (Alaghmandfard and Ghandi, 2022). Among reported different heterostructures including ZnO/g-C_3N_4 (Jang et al., 2019; N. Zhang et al., 2016), iron oxide/g-C_3N_4 (M. Wang et al., 2015; Ye et al., 2013), WO_3/g-C_3N_4 (C. Cheng et al., 2017; Xiao Zhang et al., 2020), tin oxide/g-C_3N_4 (Seza et al., 2018; Zang et al., 2014), V_2O_5/g-C_3N_4 (Jayaraman et al., 2015; Q. Liu et al., 2015) etc. Review articles have been published addressing new developments in using g-C_3N_4 for photocatalysis. Yang *et al.*(J. Yang et al., 2022) reviewed the enhanced photocatalysis resulting from the fabrication of defects in g-C_3N_4 while Jiang *et al.* (L. Jiang et al., 2021) reviewed the strategies reported to broaden the light absorption of g-C_3N_4 in the near infra-red region. In this chapter, research works reported on using TiO_2 coupled to g-C_3N_4 as visible active photocatalysts for environmental applications are reviewed.

Wei et al. reported the synthesis of mesoporous TiO_2/g-C_3N_4 microspheres and their photocatalytic activity on the degradation of phenol under visible light (H. Wei et al., 2017b). Mesoporous TiO_2 microspheres were synthesized by a solvothermal assisted method using titanium(IV) isopropoxide as the titanium precursor and mesoporous TiO_2/g-C_3N_4 microspheres, TOCN-x, (x-volume of cyanamide solution used in mL) were prepared by nanocoating procedure in which mesoporous TiO_2 microspheres were dispersed in variable volumes of aqueous cyanamide, the precursor of C_3N_4. Mesoporous g-C_3N_4 have been made via nano casting procedure, where premade SBA-15 was dispersed in an aqueous cyanamide solution followed by drying and calcination at 550 °C for 4 h in N_2 atmosphere. The silica template was removed by treating with NH_4HF_2/HCl. The shape and the size of the synthesized mesoporous TiO_2 microspheres of a diameter of about 2 μm did not change upon the formation of g-C_3N_4 in TOCN-1 and TOCN-2, without any g-C_3N_4 aggregations at the outer surface (Fig. 11(a) and (c), respectively) and the open porous structure (of TOCN-1) remained visible (Fig. 11(b)). However, aggregated nanoparticles resulting from the excess g-C_3N_4 were present on the surface in the composites with higher g-C_3N_4 loadings like TOCN-2 (Fig. 11(d)). As revealed by the TEM (Fig. 11(e)) and the HRTEM images of TOCN-1, at the interface of TiO_2/g-C_3N_4, the (101) plane of the anatase phase of TiO_2 (Fig. 11(f)) corresponds to an interlayer spacing of 3.1 Å is in close proximity to the (110) plane of g-C_3N_4 (Fig. 11(g)) indicating the successful formation of TiO_2/g-C_3N_4 heterostructure. According to the UV-Visible diffuse reflectance spectra, the light absorption of the composites shifted to the visible range compared to pure TiO_2 which the light absorption was limited to the UV range and showed a higher absorption than pure g-C_3N_4. The resulted band gaps of TiO_2, TOCN-1, TOCN-2 and g-C_3N_4 were 3.2, 1.5, 1.7 and 2.7 eV, respectively. Photoluminescence spectra have been acquired to study the separation of photogenerated charge carriers and pure TiO_2 exhibited a band in the range of 350–420 nm appeared due to

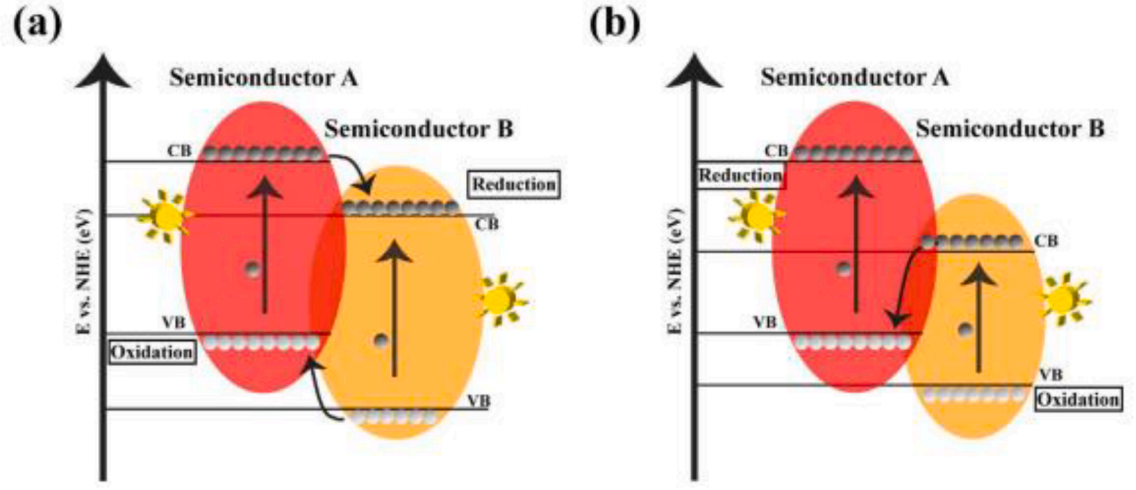

Fig. 10. The most common heterojunctions fabricated when g-C_3N_4 is coupled to metal oxides (a) type II heterojunction (b) Z-scheme heterojunction. Figure adapted from ref. (Alaghmandfard & Ghandi, 2022).

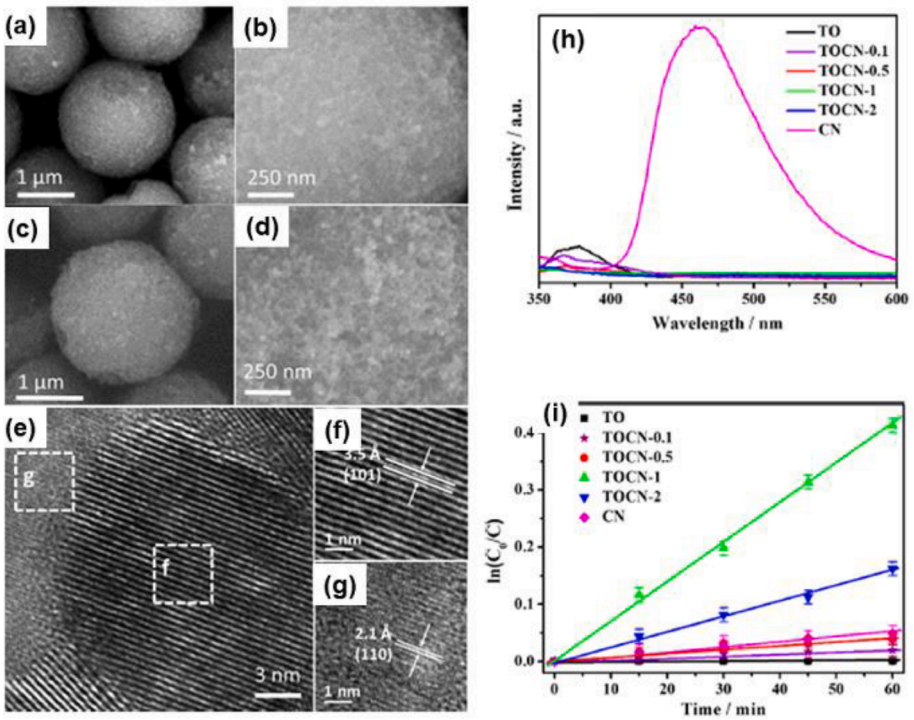

Fig. 11. SEM images of (a), (b) TOCN-1 (c), (d) TOCN-2 (e) TEM image of TOCN-1 showing the TiO_2-g-C_3N_4 interface, HRTEM images of (f) anatase TiO_2 (g) g-C_3N_4, (h) Photoluminescence spectra of (i) Photocatalytic decomposition of phenol over, TO, TOCN-0.1, TOCN-0.5, TOCN-1, TOCN-2, CN. Figure adapted from ref. (H. Wei et al., 2017).

the band-band emission and excitonic fluorescence resulting from surface oxygen vacancies and defects. Peaks with less intensity were observed for TOCN in the same range suggesting less recombination of electrons and holes but the broad peak of g-C_3N_4 centered at 460 nm with high intensity indicated the possible recombination of the photogenerated electron hole pairs (Fig. 11(h)). Photocatalytic activity of the synthesized catalysts has been evaluated on the degradation of phenol under the irradiation generated by a 500 W Hg (Xe) globe (Oriel) with a Schott filter (cutoff $\lambda < 420$ nm) as the visible light source (light intensity: 8.5 mW cm^{-2}). TOCN-1 and TOCN-2 showed higher rate constants (Fig. 11(i)) in degrading phenol than g-C_3N_4 due to the lower band gap resulting due to doping of N to TiO_2 which created an energy level (N 2p) above the valence band of TiO_2 as revealed by the XPS analysis and hence both TiO_2 and g-C_3N_4 species were visible active. Moreover, the fast transport of the reactant phenol and photodegraded products through the mesoporous structure with pore channels of larger diameter also contributed to the higher photocatalytic activity. Further, it has been found that photogenerated electrons are mainly responsible for the radical formation as revealed by the reduction in the photocatalytic activity in the presence of *t*-butanol which acted as a radical scavenger than the reduction in the activity resulting when EDTA-2Na was used as the hole scavenger because hydroxyl radicals are generated from the photoexcited electrons and oxygen radicals from the photogenerated holes. The proposed mechanism for charge transfer is illustrated in scheme 3. Photogenerated electrons at the CB band of g-C_3N_4 transfer to the CB of *N*-doped TiO_2 through the interface of the heterostructure. Holes at the N 2p substitutional level could migrate to the VB of g-C_3N_4 enhancing the charge separation. Further, exciting electrons in the CB of N doped TiO_2 and g-C_3N_4 convert O_2 to oxygen radicals which then oxidize phenol and the holes at the VB of N doped TiO_2produce hydroxyl radicals also contribute to the degradation of phenol molecules (H. Wei et al., 2017b). Further, the photodegradation of phenol has been reported in different studies using TiO_2/g-C_3N_4 thin films (Z. Wei et al., 2017a), TiO_2/g-C_3N_4 heterostructures (Qu et al., 2022), g-C_3N_4-Ti^{3+}/TiO_2 nanotube arrays (W. Liao et al., 2015),

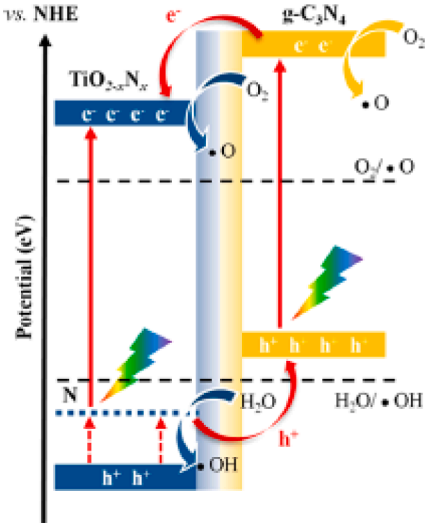

Scheme 3. Mechanism of charge transfer at the heterojunction of TiO_2 – g-C_3N_4 under visible light exposure. Scheme adapted from ref. (Z. Wei et al., 2017).

macroporous TiO_2 on B-doped/g-C_3N_4 (Behera et al., 2021), g-C_3N_4/TiO_2 composites (Miranda et al., 2013; Xueqin Wang et al., 2018c), highly ordered TiO_2 nanotube arrays wrapped with g-C_3N_4 (H. Wang et al., 2018b), TiO_2/Co-doped g-C_3N_4 (L. Zhou et al., 2017) etc.

Jo et al. studied the effect of morphology of the TiO_2 nanomaterial in TiO_2/g-C_3N_4 on photocatalytic activity for the degradation of a pharmaceutical, isoniazid (ISN) under UV irradiation (Jo & Natarajan, 2015). The morphology of the TiO_2 nanomaterial varied as nanoparticles (TNP) and nanotubes (TNT). TNT was synthesized by a hydrothermal method using TNP as the starting material. TNT degraded 73.3 % of ISN, while only 56.3 % of ISN was degraded by TNP due to the

higher surface area of TNT which led to higher adsorption of ISN to TNT (4 %) compared to TNP (0.3 %). Degradation of ISN in the presence of g-C_3N_4 was only 13.5 % which was lesser than for both TNT and TNP as g-C_3N_4 is only visible sensitive and TiO_2 nanomaterials absorb UV irradiation provided. The photocatalytic activity increased with increasing loading of g-C_3N_4 up to 5 % coupled to TNP (79.5 %). The higher photocatalytic activity was attributed to the proper contact of TNP and g-C_3N_4, reduced band gap and higher surface area (60.01 m^2/g), while the photocatalytic activity decreased with further increments of g-C_3N_4 due to the shielding effect of g-C_3N_4. Similarly, the photocatalytic activity was increased with increasing loading of g-C_3N_4 when coupled to TNT, where the maximum of 90.8 % was reported with 3 % g-C_3N_4, while the activity decreased with further increments as 77.9, 75.1 and 74.4 % for 5, 7 and 10 % loadings of g-C_3N_4. At higher g-C_3N_4 loadings, g-C_3N_4 tends to block the TNT limiting the light reaching the TNT resulting in low production of $OH^{\bullet}$ and $O_2^{\bullet-}$ radicals which lead to a reduction in the ISN degradation. Photocatalytic degradation of ISN by g-C_3N_4 coupled to TNT is greater than that of g-C_3N_4 coupled to TNP due to the high surface area of TNT which provides a larger number of active sites for the adsorption of ISN and produces a higher concentration of $OH^{\cdot}$ (Jo & Natarajan, 2015).

Similarly, Lu et al. reported the solvothermal assisted synthesis of TiO_2 nanorods on g-C_3N_4 as efficient photocatalysts for the degradation of Rhodamine B and reduction of Cr(VI) under visible light (Lu et al., 2017) as they effectively prohibit the electron hole pair recombination due to the charge transfer from g-C_3N_4 to TiO_2 nanorods. Shen et al. (Shen et al., 2017) reported the synthesis of black TiO_2 nanobelts/g-C_3N_4 sheets via the hydrothermal method where treatment with $NaBH_4$ at higher temperatures produces black nanobelts. They were photocatalytically active on hydrogen production (555.8 μmol $h^{-1}g^{-1}$) and could degrade 95.1 % of methyl orange (Shen et al., 2017). Arjum et al. also reported the synthesis of g-C_3N_4 coupled to TiO_2 nanotubes and they were capable of photodegrading 96.6 % of 2-chlorophenol (Anjum et al., 2018). Recently, g-C_3N_4 coupled to TiO_2 nanorods have been reported to be effective in photodegrading ciprofloxacin (K. Hu et al., 2020), phenol (Qi et al., 2020), Rhodamine B (Hao et al., 2017a) etc. A similar study was reported by Monga et al. (Monga & Basu, 2019) where they also studied the effect of morphology of TiO_2 on photocatalytic activity of g-C_3N_4/TiO_2 nanocomposite for the degradation of Rhodamine B in visible light (65 W CFL lamp, Phillips, K > 400 nm with an intensity of 125 W/m^2). TiO_2 nanorods, nanotubes and nanospheres have been synthesized by using titanium tetraisopropoxide, Degussa P25, and titanium butoxide as the chemical precursors. Morphology of the C_3N_4/TiO_2 nanotube, nanospheres and nanorods are shown in Fig. 12(a–c), respectively. The band gap calculated from the DRS data for g-C_3N_4 coupled to TiO_2 nanotubes, nanorods and nanospheres, are 2.0, 2.32, and 2.8 eV, respectively. The surface areas obtained for them are 137.1, 126.1, and 81.1 m^2/g, respectively. g-C_3N_4/TiO_2 nanotubes have shown the highest photocatalytic rate (0.0403 min^{-1}) followed by g-C_3N_4 coupled to TiO_2 nanorods (0.0359 min^{-1}), P25 (0.0217 min^{-1}), nanospheres (0.0175 min^{-1}) as given in Fig. 12 (d). The resulted photocatalytic activity of g-C_3N_4 coupled to TiO_2 nanotubes has been attributed to improved light absorption in the visible range and the high surface area (Monga & Basu, 2019). The photocatalytic efficiency decreased in the presence of DMSO and ascorbic acid which are electron and superoxide scavengers, respectively, indicating their importance in the degradation reaction, while the efficiency was not affected significantly by adding methanol indicating the least contribution of holes to the degradation reaction as shown in Fig. 12(e). Degradation mechanism which shows the contribution of the reactive species to the degradation of Rhodamine B is given in Fig. 12(f)(Monga & Basu, 2019). g-C_3N_4/TiO_2 nanocomposites have been reported to be effective in photodegrading Rhodamine B by other studies as well (Hao et al., 2017b; Sharma et al., 2017).

Hao et al. (Hao et al., 2017b) studied the photocatalytic activity of g-C_3N_4/TiO_2 heterojunction photocatalysts synthesized by hydrothermal method, on the degradation of Rhodamine B under visible light generated by a 350 W xenon arc lamp with UV cut off filter (420 nm). The weight of melamine, the precursor for the synthesis of g-C_3N_4 was mixed with $TiCl_4$ was varied as 0.5, 1, 2, 3, and 4 g and the composites synthesized were abbreviated as TC0.5, TC1, TC2, TC3, and TC4, respectively. Photocatalytic activity was varied as TC0.5 < TC1 < TC2 < TC3 > TC4 as given in Fig. 13. Photocatalytic activity of TC 3 is the highest among the composites synthesized and is 18.7 times higher than pure TiO_2 and 3.5 greater than pure g-C_3N_4. The obtained highest activity in the presence of TC3 is due to the high surface area it possesses (115.6 m^2/g), narrower band gap (2.97 eV) leading to increase absorption of visible light and the heterostructure formed, in which the band alignment minimizes the electron hole pair recombination(Jian Xu et al., 2015; J. Yu et al., 2013). Meanwhile, the photocatalytic activity of TC 4 decreased because excessive incorporation of melamine decreased the surface area and destruct the heterostructure between TiO_2 and g-C_3N_4

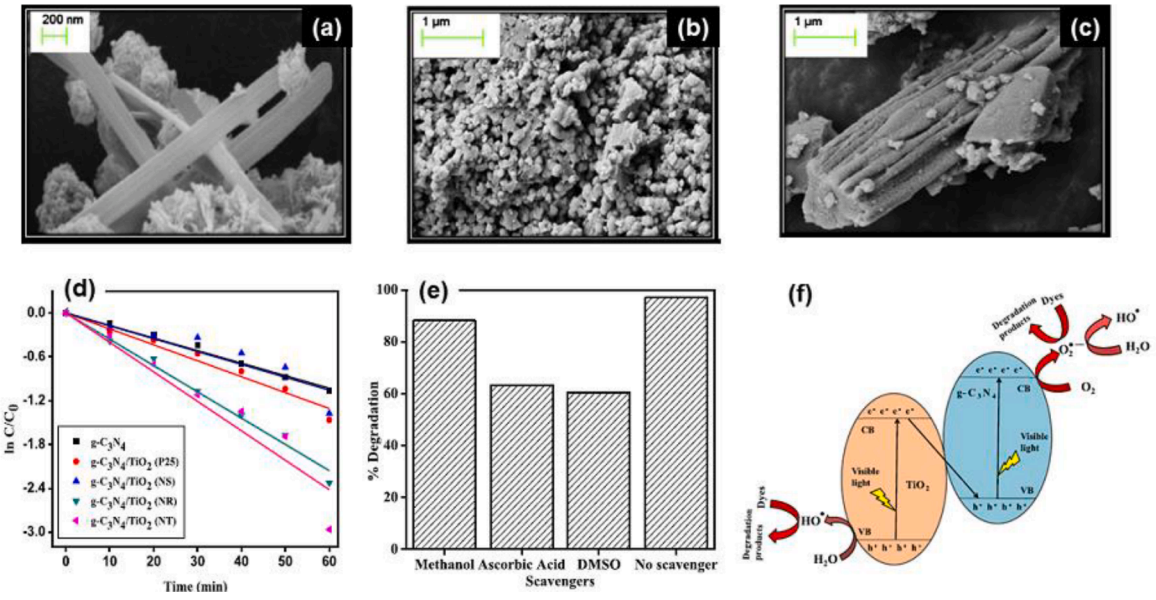

Fig. 12. FESEM images of g-C_3N_4/TiO_2 (a) Nanotubes (b) Nanospheres (c) Nanorods (d) Kinetics analysis (e) scavenger study for photodegradation of Rhodamine B (f) scheme indicating the photodegradation mechanism. Figure adapted from. Ref. (Monga & Basu, 2019).

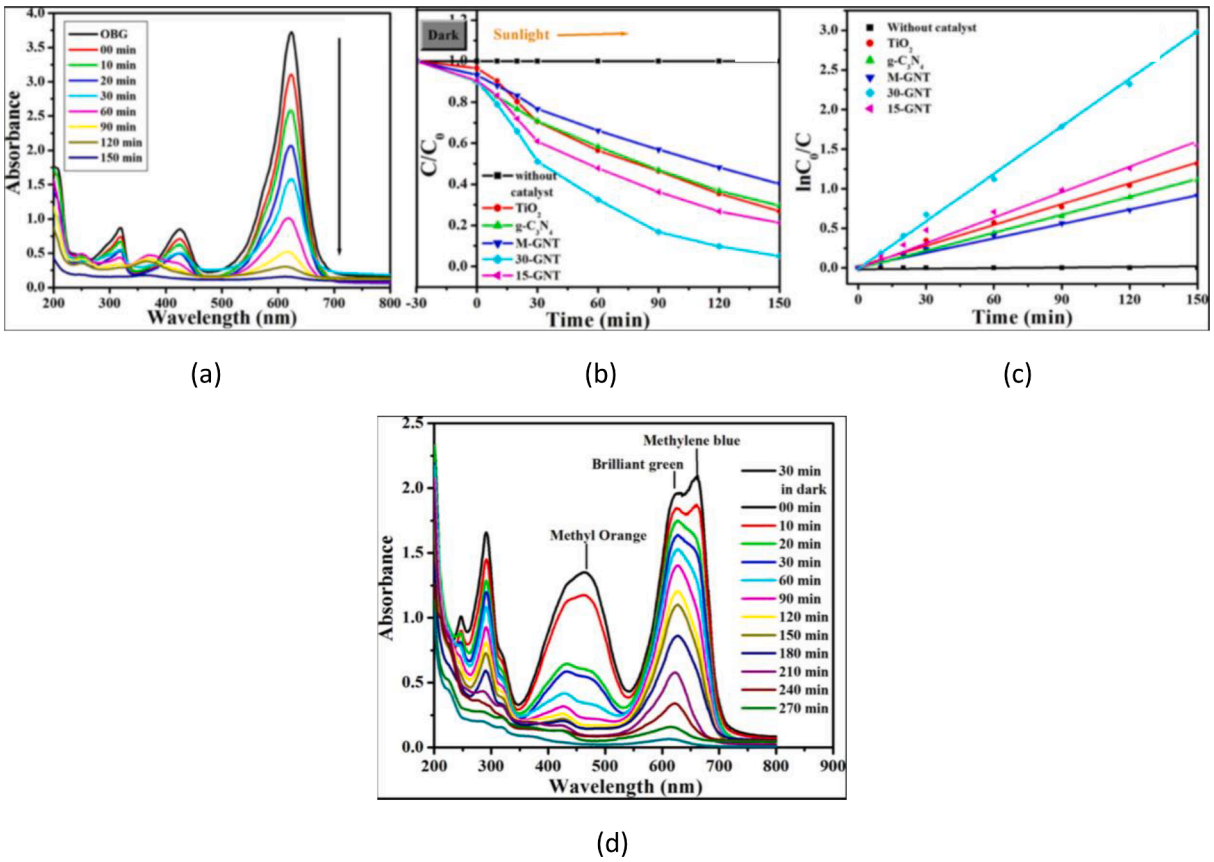

Fig. 13. (a) Time resolve UV-Visible spectra of brilliant green (b) Kinetics plot of C/C_o vs time, plot (d) Time resolve UV-Visible spectra of dye mixture in the presence of 30 GNT. Figure adapted from ref. (Sutar et al., 2020). (For interpretation of the references to colour in this figure legend, the reader is referred to the web version of this article.)

(R. Hao et al., 2016; Hao et al., 2017b). Sutar et al. reported the effective use of g-C_3N_4/TiO_2 nanocomposites for the photodegradation of bisphenol A, Brilliant green, and a mixture of Brilliant green, methylene blue, and methyl orange under sunlight (Sutar et al., 2020). Titanium-tetra isopropoxide has been used as the titanium source and a mixture of urea and thiourea has been used as the raw materials for g-C_3N_4. Synthesized g-C_3N_4 was coupled to TiO_2 during the synthesis of TiO_2 hydrothermally in two different molar ratios as g-C_3N_4 to TiO_2, 15:85 and 30:70 which are denoted as 15 GNT and 30 GNT, respectively. The absorption edge of the synthesized nanocomposites shifted to the visible range compared to pure TiO_2 due to the presence of g-C_3N_4 resulting in lower band gaps of 2.9 and 3.16 eV, for 15GNT and 30 GNT, respectively, compared to pure TiO_2 (3.3 eV). Among the tested photocatalysts, 30 GNT (19.85×10^{-3} min^{-1}) was effective than 15GNT (12.42×10^{-3} min^{-1}), pure TiO_2 (9.32×10^{-3} min^{-1}) and g-C_3N_4 (7.72×10^{-3} min^{-1}) due to lower crystallite size (11.4 nm), low band gap (2.9 eV) and effective charge separation (Fig. 13(a–c)). The behaviour of the photocatalysts was similar in degrading bisphenol A. Further, 30 GNT was effective in degrading all dyes in a mixture of Brilliant green, methylene blue, and methyl orange (Fig. 13(d)) (Sutar et al., 2020).

Du et al. (Du et al., 2020) reported the synthesis of TiO_2/g-C_3N_4 using melamine as the precursor of g-C_3N_4 and commercially available TiO_2. They were mixed in different weight ratios as 2.5, 5, 10, 20, 30, 40, and 50 % and were coupled via sonication followed by calcination. Their effect on photodegrading acetaminophen was evaluated under visible light generated from a 300 W xenon lamp. TiO_2 coupled with 5 % g-C_3N_4 showed the highest photocatalytic activity. The conversion was enhanced from 33.2 % to 99.3 %, and the rate constant increased 13 times upon the addition of persulfate. The photocatalytic activity was low at low content of g-C_3N_4, g-C_3N_4 cannot provide sufficient photoinduced carriers for persulfate to be activated and at a high percentage of g-C_3N_4 again the photocatalytic activity was low due to insufficient content of TiO_2, photoinduced carriers generated by g-C_3N_4 cannot be transferred into TiO_2 and decrease the charge separation. TiO_2/g-C_3N_4 was effective in photodegrading other micropollutants such as phenol, bisphenol A and carbamazepine as well. Further, the photodegradation of acetaminophen reduced from 100 % to 88.3 % and 94.5 % once the medium of the reaction carried out was changed from ultrapure water to tap water and lake water as the other organic matter compete with acetaminophen and hence the photocatalyst has nonselective photocatalytic properties (Du et al., 2020).

TiO_2/g-C_3N_4 has shown in be effective in photodegrading methylene blue (Bairamis et al., 2019; H. Liu et al., 2019), methyl orange (Kuldeep et al., 2021; Q. Li et al., 2013; Mohini & Lakshminarasimhan, 2016), rhodamine B (L. Ma et al., 2018; M. Sharma et al., 2017), diclofenac sodium (John et al., 2021), Indigo Carmine (Toghan et al., 2021) etc. Table 5 summarizes the synthesis method, textural parameters, morphology and the photocatalysis of TiO_2/g-C_3N_4 reported in the literature.

2.2.1.2. Advantages and disadvantages. Pure TiO_2 with anatase or rutile crystal phases is only UV active and hence the applicability of pure TiO_2 for photocatalysis especially for environmental remediation is limited. However, the use of TiO_2 in visible light is significantly enhanced when coupled to g-C_3N_4 due to the visible light sensitivity of g-C_3N_4 and transfer of photoexcited electrons to the CB of TiO_2 from the CB of g-C_3N_4 due to the potential difference. On the other hand, the prominent disadvantage of using g-C_3N_4 as a photocatalyst, electron hole pair recombination is minimized once coupled with TiO_2 due to the efficient charge transfer. The synthesis of g-C_3N_4 is straightforward as requires

Table 5
A summary of TiO_2/g-C_3N_4 nanocomposites and their photocatalytic activity.

Precursor of g-C_3N_4	Synthetic method	Morphology of TiO_2	Surface area (m^2/g)	Band Gap (eV)	Light Source	Pollutant	Pollutant Concentration (mg/L)	Weight of the Catalyst (mg)	Rate (min^{-1})/ Conversion	Performance compared to TiO_2	Performance compared to g-C_3N_4	Reference
Cyanamide	Solvothermal	Microspheres	64.4	1.5	500 W Hg (light intensity: 8.5 mW cm^{-2})	Phenol	10	80	6.8×10^{-3}	–	8.5 times	(H. Wei et al., 2017)
Melamine	Grinding followed by calcination	Disc shape	92.5	2.27	300 W Xe lamp	Phenol	20	30	1.63×10^{2} μmol g^{-1} $1\,h^{-1}$ *	–	141.67 times	(Qu et al., 2022)
						p-nitrophenol			1.15×10^{2} μmol $g^{-1}h^{-1}$ *		500 times	
						o-cresol			1.43×10^{2} μmol $g^{-1}h^{-1}$ *		–	
						p-cresol			1.45×10^{2} μmol $g^{-1}h^{-1}$ *		–	
Melamine	Calcination	Nanotubes	–	2.78	11 W incandescent lamp (Intensity of 3 mW cm^{-2})	Phenol	10	–	74 %	4 times	–	(W. Liao et al., 2015)
Melamine	Wetness impregnation	Nanoparticles	60.01	3.14	–	Isoniazid	50	100	6.93×10^{-3}	1.11 times	3.36 times	(Jo & Natarajan, 2015)
		Nanotubes	58.54	3.27					8.33×10^{-3}	1.19 times	4.04 times	
Urea	Solvothermal	Nanorods	88.64	3.09	Xe lamp	Rhodamine B	20		16.98×10^{-3}	3.04 times	1.88 times	(Lu et al., 2017)
						Cr(VI)	50		38.33×10^{-3}	4.38 times	2.72 times	
Melamine	Grinding followed by calcination	Nanobelts	29.3	2.32	300 W Xeon-lamp with a 420 nm cutoff filter	Methyl Orange	10	30	1.53×10^{-2}	9.56 times	6.12 times	(Shen et al., 2017)
Melamine	Sonication followed by drying	Nanorods	–	2.95	500 W Xenon lamp	Ciprofloxacin	0.02	10	3.66×10^{-2}	2.3 times	7.5 times	(K. Hu et al., 2020)
Urea	Sonication followed by drying	Nanotubes	137.1	2.0	65 W 205 CFL lamp, Phillips, k > 400 nm with intensity of 125 W/m^2	Rhodamine B	5	2	4.03×10^{-2}	–	2.33 times	(Monga & Basu, 2019)
		Nanorods	126.1	2.32					3.59×10^{-2}	–	2.07 times	
		Nanospheres	81.1	2.8					1.75×10^{-2}	–	1.01 times	
Melamine	Hydrothermal	–	115.6	2.97	350 W xenon arc lamp with UV-cutoff filter (420 nm)	Rhodamine B	4.8	40	36.7×10^{-3}	18.7 times	3.5 times	(R. Hao et al., 2017)
Urea and Thiourea	Hydrothermal	–	–	2.7	Sunlight	Brilliant Green	20	100	19.85×10^{-3}	6.1 times	2.57 times	(Sutar et al., 2020)
						Bisphenol A			30.32×10^{-3}	1.92 times	3.73 times	
Urea	Grinding followed by calcination	Flower-like microspheres	115.4		30 W Fluorescent lamp	Methyl Orange	10	100	6.93×10^{-1}	7 times	–	(C. Hu et al., 2019)
Melamine	Sonication followed by Calcination	Nanoparticles	–	2.34	300 W xenon lamp with a 400 nm cutoff filter	Acetaminophen	5	50	1.615×10^{-1}	30 times	15 times	(Du et al., 2020)
Urea	Wet impregnation	Nanoparticles	18.44	3.05	1000 W halogen lamp	Diclofenac sodium	5	300	93.5	1.87 times	1.2 times	(John et al., 2021)
Carbonyl diamide	Sonication followed by Calcination	Nanoparticles	155	2.97	OSRAM lamp 58 IM/W	Indigo Carmine	50	50	2.98×10^{-2}	7 times	4.6 times	(Toghan et al., 2021)

* Unit was not unified as sufficient data were not available.

only annealing of the precursor and does not involve multiple steps.

The reusability of the nanocomposites is high favouring their applicability. Despite the light absorption being enhanced, charge separation is improved and increase the rate of photocatalytic reaction there are disadvantages associated with TiO_2/g-C_3N_4 composites. Adsorption of the pollutants is a crucial parameter that governs the rate of reaction but once g-C_3N_4 is used as the adsorption is comparatively lower, a low photocatalysis was resulted. Moreover, the yield of g-C_3N_4 produced by annealing the precursors including urea, melamine, thiourea, and cyanamide is very low and hence large-scale production of g-C_3N_4-based photocatalysis is a challenge using g-C_3N_4 as a photocatalyst is not cost-effective. During the synthesis, coupling of TiO_2 and g-C_3N_4 requires a hydrothermal method which requires special lab equipment.

3. Challenges and opportunities

There a quite a few challenges associated with using TiO_2 coupled with carbon-based materials as photocatalysts. The main challenge is that carbon material masks the penetration of light to the photocatalyst and hence the concentration of the radicals formed which are responsible for the degradation of pollutants. Further, when the photocatalysis of pure TiO_2 is compared with the TiO_2 coupled with the carbon material many researchers have directly compared the photocatalytic activity per given weight of the catalyst ignoring the fact that in a given weight of the composite the weight of the actual catalyst (TiO_2) is a constant and the weight of the carbon material is varied. Therefore, the rate of photocatalysis or the conversion should be calculated considering the weight of the catalyst in the particular weight of the total composite. However, this doesn't apply to TiO_2/g-C_3N_4 as g-C_3N_4 is also a component of the photocatalyst. Further, the dark or opaque colour caused by the black colour of the carbon-based material interferes with the measurements collected by the UV-Visible spectrophotometer.

Photocatalysts of TiO_2 coupled with carbon-based materials are not only applicable for the degradation of pollutants in wastewater but also could be used to generate H_2 from water splitting which is a sustainable energy source. Further, these composites could be used as an antimicrobial agent to inhibit the growth of bacteria and fungi, mainly.

4. Recommendations and future outlook

As described above coupling of TiO_2 with carbon-originated materials have shown to be promising photocatalysts in degrading pollutants that are released from different anthropogenic activities. However, in the future researchers can further improve the activity and enhance the efficiency of the photocatalysts. As reported the efficiency in degrading the pollutants under visible light is lesser than that under UV light because TiO_2 is UV sensitive. Therefore, to improve the activity under visible light, TiO_2 could be modified to increase the absorption of visible light. TiO_2 doped with transition metals like Fe, Cu, Mn etc., and non-metals such as N, C, S etc. could be coupled with carbon-based materials. Further, to enhance the visible light sensitivity TiO_2 could be coupled with visible light sensitive semiconductors such as CuO, Fe_2O_3, WO_3 etc. and such composite could be coupled further with the carbon-based materials.

Interestingly, TiO_2 could be decorated with noble metal nanoparticles such as Ag or Au could be coupled to carbon-based material to improve the visible light absorption due to the localized plasmon effect of the noble nanoparticles. Creating Ti^{3+} on TiO_2 and then coupling it with carbon material would also improve the visible light sensitivity. Moreover, coupling TiO_2 with more than one type of carbon material would also enhance the activity. TiO_2 coupled with g-C_3N_4 or with CNT could be deposited on AC to improve the removal of the pollutants both via adsorption and photocatalysis. Further, TiO_2 coupled to catalytically graphitized carbon has not been popularly reported. Graphitic carbon could be easily prepared by catalytic graphitization of carbon sources like sucrose and cellulose which could be extracted from natural and waste materials. Arrangement of the atomic layers to produce turbostratic carbon would enhance the adsorption of the pollutants and improve the photocatalysis via minimizing the charge carrier recombination and turbostratic carbon itself would produce the electrons and holes upon exposure to visible light. Therefore, there are different new approaches still available in the field which could be researched in the future.

5. Conclusions

TiO_2 coupled with carbon-based materials has emerged as a new avenue for the fabrication of efficient photocatalysts to degrade pollutants in wastewater. Coupling TiO_2 with activated carbon, carbon nanotubes and graphene derivatives like graphene oxide and reduce graphene oxide enhance the photocatalytic activity by providing adsorption sites to the pollutants and separating the charge carriers minimizing the electron hole pair recombination. g-C_3N_4 being different to the others, act as a visible light-sensitive semiconductor creating either type II or Z-scheme heterojunction with TiO_2 enhancing the photocatalytic activity. Visible light absorption is increased in TiO_2 coupled to carbon-based materials increasing the photodegradation of pollutants in the visible light. Though carbon-based materials improve the overall photocatalytic activity, at higher concentrations they mask the TiO_2 photocatalyst producing a smaller number of photogenerated electrons and holes leading to lower photocatalytic activity. TiO_2 coupled to g-C_3N_4 enhances the photodegradation activity only at the correct ratio between TiO_2 and g-C_3N_4 which favours the formation of the heterostructure. Therefore, TiO_2 coupled with above mentioned carbon-based materials at the correct ratio would enhance the photocatalytic activity to degrade pollutants in wastewater.

Declaration of Competing Interest

The authors declare that they have no known competing financial interests or personal relationships that could have appeared to influence the work reported in this paper.

Data availability

No data was used for the research described in the article.

Funding

This research was supported by the Accelerating Higher Education Expansion and Development (AHEAD) Operation of the Ministry of Higher Education funded by the World Bank.

References

Adly, M.S., El-Dafrawy, S.M., El-Hakam, S.A., 2019. Application of nanostructured graphene oxide/titanium dioxide composites for photocatalytic degradation of rhodamine B and acid green 25 dyes. Journal of Materials Research and Technology 8 (6), 5610–5622. https://doi.org/10.1016/J.JMRT.2019.09.029.

Akbal, F., 2005. Photocatalytic degradation of organic dyes in the presence of titanium dioxide under UV and solar light: Effect of operational parameters. Environmental Progress 24 (3), 317–322. https://doi.org/10.1002/EP.10092.

Akpan, U.G., Hameed, B.H., 2009. Parameters affecting the photocatalytic degradation of dyes using TiO2-based photocatalysts: A review. Journal of Hazardous Materials 170 (2–3), 520–529. https://doi.org/10.1016/J.JHAZMAT.2009.05.039.

Alaghmandfard, A., & Ghandi, K. (2022). A Comprehensive Review of Graphitic Carbon Nitride (g-C3N4)–Metal Oxide-Based Nanocomposites: Potential for Photocatalysis and Sensing. *Nanomaterials 2022, Vol. 12, Page 294*, *12*(2), 294. https://doi.org/10.3390/NANO12020294.

Al-Maqdi, K. A., Elmerhi, N., Athamneh, K., Bilal, M., Alzamly, A., Ashraf, S. S., & Shah, I. (2021). Challenges and Recent Advances in Enzyme-Mediated Wastewater Remediation—A Review. *Nanomaterials 2021, Vol. 11, Page 3124*, *11*(11), 3124. https://doi.org/10.3390/NANO11113124.

Andriantsiferana, C., Mohamed, E.F., Delmas, H., 2014. Photocatalytic degradation of an azo-dye on TiO2/activated carbon composite material. Environmental Technology 35 (3), 355–363. https://doi.org/10.1080/09593330.2013.828094.

Anjum, M., Kumar, R., Abdelbasir, S.M., Barakat, M.A., 2018. Carbon nitride/titania nanotubes composite for photocatalytic degradation of organics in water and sludge: Pre-treatment of sludge, anaerobic digestion and biogas production. Journal of Environmental Management 223, 495–502. https://doi.org/10.1016/J.JENVMAN.2018.06.043.

Asencios, Y.J.O., Lourenço, V.S., Carvalho, W.A., 2022. Removal of phenol in seawater by heterogeneous photocatalysis using activated carbon materials modified with TiO2. Catalysis Today 388–389, 247–258. https://doi.org/10.1016/J.CATTOD.2020.06.064.

Ateia, M., Apul, O.G., Shimizu, Y., Muflihah, A., Yoshimura, C., Karanfil, T., 2017. Elucidating Adsorptive Fractions of Natural Organic Matter on Carbon Nanotubes. Environmental Science and Technology 51 (12), 7101–7110. https://doi.org/10.1021/ACS.EST.7B01279/SUPPL_FILE/ES7B01279_SI_001.PDF.

Awfa, D., Ateia, M., Fujii, M., Yoshimura, C., 2019. Novel Magnetic Carbon Nanotube-TiO2 Composites for Solar Light Photocatalytic Degradation of Pharmaceuticals in the Presence of Natural Organic Matter. Journal of Water Process Engineering 31, 100836. https://doi.org/10.1016/J.JWPE.2019.100836.

Bairamis, F., Konstantinou, I., Petrakis, D., & Vaimakis, T. (2019). Enhanced Performance of Electrospun Nanofibrous TiO2/g-C3N4 Photocatalyst in Photocatalytic Degradation of Methylene Blue. *Catalysts 2019, Vol. 9, Page 880*, *9* (11), 880. https://doi.org/10.3390/CATAL9110880.

Balayeva, N.O., Fleisch, M., Bahnemann, D.W., 2018. Surface-grafted WO3/TiO2 photocatalysts: Enhanced visible-light activity towards indoor air purification. Catalysis Today 313, 63–71. https://doi.org/10.1016/J.CATTOD.2017.12.008.

Barakat, M.A., Kumar, R., Almeelbi, T., Al-Mur, B.A., Eniola, J.O., 2022. Sustainable visible light photocatalytic scavenging of the noxious organic pollutant using recyclable and reusable polyaniline coupled WO3/WS2 nanohybrid. Journal of Cleaner Production 330, 129942. https://doi.org/10.1016/J.JCLEPRO.2021.129942.

Bedia, J., Monsalvo, V.M., Rodriguez, J.J., Mohedano, A.F., 2017. Iron catalysts by chemical activation of sewage sludge with FeCl3 for CWPO. Chemical Engineering Journal 318, 224–230. https://doi.org/10.1016/J.CEJ.2016.06.096.

Bedia, J., Belver, C., Ponce, S., Rodriguez, J., Rodriguez, J.J., 2018. Adsorption of antipyrine by activated carbons from FeCl3-activation of Tara gum. Chemical Engineering Journal 333, 58–65. https://doi.org/10.1016/J.CEJ.2017.09.161.

Behera, A., Babu, P., Parida, K., 2021. Growth of macroporous TiO2 on B-doped g-C3N4 nanosheets: a Z-scheme photocatalyst for H2O2 production and phenol oxidation under visible light. Inorganic Chemistry Frontiers 8 (6), 1489–1499. https://doi.org/10.1039/D0QI01327G.

Boreen, A.L., Arnold, W.A., McNeill, K., 2004. Photochemical fate of sulfa drugs in then aquatic environment: Sulfa drugs containing five-membered heterocyclic groups. Environmental Science and Technology 38 (14), 3933–3940. https://doi.org/10.1021/ES0353053/SUPPL_FILE/ES0353053SI20040419_023951.PDF.

Briche, S., Derqaoui, M., Belaiche, M., El Mouchtari, E.M., Wong-Wah-Chung, P., Rafqah, S., 2020. Nanocomposite material from TiO2 and activated carbon for the removal of pharmaceutical product sulfamethazine by combined adsorption/photocatalysis in aqueous media. Environ Sci Pollut Res 27 (20), 25523–25534.

Cao, N., Yue, C., Lin, Z., Li, W., Zhang, H., Pang, J., Jiang, Z., 2021. Durable and chemical resistant ultra-permeable nanofiltration membrane for the separation of textile wastewater. Journal of Hazardous Materials 414, 125489. https://doi.org/10.1016/J.JHAZMAT.2021.125489.

Caturla, F., Molina-Sabio, M., Rodríguez-Reinoso, F., 1991. Preparation of activated carbon by chemical activation with ZnCl2. Carbon 29 (7), 999–1007. https://doi.org/10.1016/0008-6223(91)90179-M.

Chai, W.S., Cheun, J.Y., Kumar, P.S., Mubashir, M., Majeed, Z., Banat, F., Ho, S.H., Show, P.L., 2021. A review on conventional and novel materials towards heavy metal adsorption in wastewater treatment application. Journal of Cleaner Production 296, 126589. https://doi.org/10.1016/J.JCLEPRO.2021.126589.

Chatterjee, M.J., Ghosh, A., Mondal, A., Banerjee, D., 2017. Polyaniline–single walled carbon nanotube composite – a photocatalyst to degrade rose bengal and methyl orange dyes under visible-light illumination. RSC Advances 7 (58), 36403–36415. https://doi.org/10.1039/C7RA03855K.

Chen, X., Zhao, X., Kong, Z., Ong, W.J., Li, N., 2018. Unravelling the electrochemical mechanisms for nitrogen fixation on single transition metal atoms embedded in defective graphitic carbon nitride. Journal of Materials Chemistry A 6 (44), 21941–21948. https://doi.org/10.1039/C8TA06497K.

Cheng, C., Shi, J., Hu, Y., Guo, L., 2017. WO3/g-C3N4 composites: one-pot preparation and enhanced photocatalytic H2 production under visible-light irradiation. Nanotechnology 28 (16), 164002. https://doi.org/10.1088/1361-6528/AA651A.

Cheng, N., Wang, B., Wu, P., Lee, X., Xing, Y., Chen, M., Gao, B., 2021. Adsorption of emerging contaminants from water and wastewater by modified biochar: A review. Environmental Pollution 273, 116448. https://doi.org/10.1016/J.ENVPOL.2021.116448.

de la Flor, M.P., Camarillo, R., Martínez, F., Jiménez, C., Quiles, R., Rincón, J., 2021. Removal of emerging pollutant dibutylhydroxytoluene from water with CNT/TiO2 catalysts in a visible LED photoreactor. Environ Sci Pollut Res 28 (19), 23720–23730.

de Oliveira Pereira, L., Marques Sales, I., Pereira Zampiere, L., Silveira Vieira, S., do Rosário Guimarães, I., & Magalhães, F. (2019). Preparation of magnetic photocatalysts from TiO2, activated carbon and iron nitrate for environmental remediation. *Journal of Photochemistry and Photobiology A: Chemistry*, *382*, 111907. https://doi.org/10.1016/J.JPHOTOCHEM.2019.111907.

Devendran, P., Selvakumar, D., Ramadoss, G., Sivaramakrishnan, R., Alagesan, T., Jayavel, R., Pandian, K., 2022. A novel visible light active rare earth doped CdS nanoparticles decorated reduced graphene oxide sheets for the degradation of cationic dye from wastewater. Chemosphere 287, 132091. https://doi.org/10.1016/J.CHEMOSPHERE.2021.132091.

Dong, Y., Shao, J., Chen, C., Li, H., Wang, R., Chi, Y., Lin, X., Chen, G., 2012. Blue luminescent graphene quantum dots and graphene oxide prepared by tuning the carbonization degree of citric acid. Carbon 50 (12), 4738–4743. https://doi.org/10.1016/J.CARBON.2012.06.002.

Du, X., Bai, X., Xu, L., Yang, L., Jin, P., 2020. Visible-light activation of persulfate by TiO2/g-C3N4 photocatalyst toward efficient degradation of micropollutants. Chemical Engineering Journal 384, 123245. https://doi.org/10.1016/J.CEJ.2019.123245.

Edelmannová, M., Lin, K.Y., Wu, J.C.S., Troppová, I., Čapek, L., Kočí, K., 2018. Photocatalytic hydrogenation and reduction of CO2 over CuO/TiO2 photocatalysts. Applied Surface Science 454, 313–318. https://doi.org/10.1016/J.APSUSC.2018.05.123.

El Golli, A., Fendrich, M., Bazzanella, N., Dridi, C., Miotello, A., Orlandi, M., 2021. Wastewater remediation with ZnO photocatalysts: Green synthesis and solar concentration as an economically and environmentally viable route to application. Journal of Environmental Management 286, 112226. https://doi.org/10.1016/J.JENVMAN.2021.112226.

El Mouchtari, E.M., Daou, C., Rafqah, S., Najjar, F., Anane, H., Piram, A., Hamade, A., Briche, S., Wong-Wah-Chung, P., 2020. TiO2 and activated carbon of Argania Spinosa tree nutshells composites for the adsorption photocatalysis removal of pharmaceuticals from aqueous solution. Journal of Photochemistry and Photobiology A: Chemistry 388, 112183. https://doi.org/10.1016/J.JPHOTOCHEM.2019.112183.

Fan, Z., Yan, J., Zhi, L., Zhang, Q., Wei, T., Feng, J., Zhang, M., Qian, W., Wei, F., 2010. A Three-Dimensional Carbon Nanotube/Graphene Sandwich and Its Application as Electrode in Supercapacitors. Advanced Materials 22 (33), 3723–3728. https://doi.org/10.1002/ADMA.201001029.

Fawzi Suleiman Khasawneh, O., Palaniandy, P., 2021. Removal of organic pollutants from water by Fe2O3/TiO2 based photocatalytic degradation: A review. Environmental Technology & Innovation 21, 101230. https://doi.org/10.1016/J.ETI.2020.101230.

Fu, X., Yang, H., Lu, G., Tu, Y., Wu, J., 2015. Improved performance of surface functionalized TiO2/activated carbon for adsorption–photocatalytic reduction of Cr (VI) in aqueous solution. Materials Science in Semiconductor Processing 39, 362–370. https://doi.org/10.1016/J.MSSP.2015.05.034.

Gar Alalm, M., Tawfik, A., Ookawara, S., 2016. Enhancement of photocatalytic activity of TiO2 by immobilization on activated carbon for degradation of pharmaceuticals. Journal of Environmental Chemical Engineering 4 (2), 1929–1937. https://doi.org/10.1016/J.JECE.2016.03.023.

Gu, C., Shannon, C., 2007. Investigation of the photocatalytic activity of TiO2–polyoxometalate systems for the oxidation of methanol. Journal of Molecular Catalysis A: Chemical 262 (1–2), 185–189. https://doi.org/10.1016/J.MOLCATA.2006.08.029.

Gu, Y., Yperman, J., Carleer, R., D'Haen, J., Maggen, J., Vanderheyden, S., Vanreppelen, K., Garcia, R.M., 2019. Adsorption and photocatalytic removal of Ibuprofen by activated carbon impregnated with TiO2 by UV–Vis monitoring. Chemosphere 217, 724–731. https://doi.org/10.1016/J.CHEMOSPHERE.2018.11.068.

Gunnagol, R.M., Rabinal, M.H.K., 2018. TiO2-Graphene Nanocomposites for Effective Photocatalytic Degradation of Rhodamine-B Dye. ChemistrySelect 3 (9), 2578–2585. https://doi.org/10.1002/SLCT.201703081.

Guo, X. P., Zang, P., Li, Y. M., & Bi, D. S. (2021). TiO2-Powdered Activated Carbon (TiO2/PAC) for Removal and Photocatalytic Properties of 2-Methylisoborneol (2-MIB) in Water. *Water 2021, Vol. 13, Page 1622*, *13*(12), 1622. https://doi.org/10.3390/W13121622.

Gupta, S.M., Tripathi, M., 2011. A review of TiO2 nanoparticles. Chin. Sci. Bull. 56 (16), 1639–1657.

Hanaor, D.A.H., Sorrell, C.C., 2011. Review of the anatase to rutile phase transformation. In *Journal of Materials Science* (Vol. 46 (4), 855–874. https://doi.org/10.1007/s10853-010-5113-0.

Hao, R., Wang, G., Tang, H., Sun, L., Xu, C., Han, D., 2016. Template-free preparation of macro/mesoporous g-C3N4/TiO2 heterojunction photocatalysts with enhanced visible light photocatalytic activity. Applied Catalysis B: Environmental 187, 47–58. https://doi.org/10.1016/J.APCATB.2016.01.026.

Hao, R., Wang, G., Jiang, C., Tang, H., Xu, Q., 2017b. In situ hydrothermal synthesis of g-C3N4/TiO2 heterojunction photocatalysts with high specific surface area for Rhodamine B degradation. Applied Surface Science 411, 400–410. https://doi.org/10.1016/J.APSUSC.2017.03.197.

Hao, J., Zhang, S., Ren, F., Wang, Z., Lei, J., Wang, X., Cheng, T., Li, L., 2017a. Synthesis of TiO2@g-C3N4 core-shell nanorod arrays with Z-scheme enhanced photocatalytic activity under visible light. Journal of Colloid and Interface Science 508, 419–425. https://doi.org/10.1016/J.JCIS.2017.08.065.

Hardiansyah, A., Budiman, W.J., Yudasari, N., Isnaeni, K., T., & Wibowo, A., 2021. Facile and Green Fabrication of Microwave-Assisted Reduced Graphene Oxide/Titanium Dioxide Nanocomposites as Photocatalysts for Rhodamine 6G Degradation. ACS Omega 6 (47), 32166–32177. https://doi.org/10.1021/ACSOMEGA.1C04966/ASSET/IMAGES/ACSOMEGA.1C04966.SOCIAL.JPEG_V03.

Haris, A., Gunawan, G., Widodo, D.S., Nuryanto, R., Lusiana, R.A., Viantikasari, M., 2019. Synthesis, Characterization of Cu, S doped TiO2 and Its Photocatalytic Activity for Degradation of Remazol Black B. Jurnal Kimia Sains Dan Aplikasi 22 (2), 47–51. https://doi.org/10.14710/JKSA.22.2.47-51.

Hu, C., E, L., Hu, K., Lai, L., Zhao, D., Zhao, W., Rong, H., 2019. Simple synthesis of 3D flower-like g-C3N4/TiO2 composite microspheres for enhanced visible-light photocatalytic activity. J Mater Sci 55 (1), 151–162.

Hu, K., Li, R., Ye, C., Wang, A., Wei, W., Hu, D., Qiu, R., Yan, K., 2020. Facile synthesis of Z-scheme composite of TiO2 nanorod/g-C3N4 nanosheet efficient for photocatalytic degradation of ciprofloxacin. Journal of Cleaner Production 253, 120055. https://doi.org/10.1016/J.JCLEPRO.2020.120055.

Hu, J., Wu, B., Chen, L., Song, C., Yang, H., Long, F., Sun, J., Chi, R., 2022. Influences of CeO2 morphology on enhanced performance of electro-Fenton for wastewater treatment. Journal of Rare Earths. https://doi.org/10.1016/J.JRE.2022.03.014.

Huang, S.H., Chen, D.H., 2009. Rapid removal of heavy metal cations and anions from aqueous solutions by an amino-functionalized magnetic nano-adsorbent. Journal of Hazardous Materials 163 (1), 174–179. https://doi.org/10.1016/J.JHAZMAT.2008.06.075.

Huang, J., Dou, L., Li, J., Zhong, J., Li, M., Wang, T., 2021. Excellent visible light responsive photocatalytic behavior of N-doped TiO2 toward decontamination of organic pollutants. Journal of Hazardous Materials 403, 123857. https://doi.org/10.1016/J.JHAZMAT.2020.123857.

Huang, Y., Chen, D., Hu, X., Qian, Y., & Li, D. (2018). Preparation of TiO2/Carbon Nanotubes/Reduced Graphene Oxide Composites with Enhanced Photocatalytic Activity for the Degradation of Rhodamine B. *Nanomaterials 2018, Vol. 8, Page 431*, *8* (6), 431. https://doi.org/10.3390/NANO8060431.

Jang, E., Kim, D.W., Hong, S.H., Park, Y.M., Park, T.J., 2019. Visible light-driven g-C3N4@ZnO heterojunction photocatalyst synthesized via atomic layer deposition with a specially designed rotary reactor. Applied Surface Science 487, 206–210. https://doi.org/10.1016/J.APSUSC.2019.05.035.

Jayaraman, T., Arumugam Raja, S., Priya, A., Jagannathan, M., Ashokkumar, M., 2015. Synthesis of a visible-light active V2O5–g-C3N4 heterojunction as an efficient photocatalytic and photoelectrochemical material. New Journal of Chemistry 39 (2), 1367–1374. https://doi.org/10.1039/C4NJ01807A.

Jiang, B., Tian, C., Pan, Q., Jiang, Z., Wang, J.Q., Yan, W., Fu, H., 2011. Enhanced photocatalytic activity and electron transfer mechanisms of graphene/TiO2 with exposed 001 facets. Journal of Physical Chemistry C 115 (48), 23718–23725. https://doi.org/10.1021/JP207624X/SUPPL_FILE/JP207624X_SI_001.PDF.

Jiang, L., Yang, J., Zhou, S., Yu, H., Liang, J., Chu, W., Li, H., Wang, H., Wu, Z., Yuan, X., 2021. Strategies to extend near-infrared light harvest of polymer carbon nitride photocatalysts. Coordination Chemistry Reviews 439, 213947. https://doi.org/10.1016/J.CCR.2021.213947.

Jiang, L., Zhou, S., Yang, J., Wang, H., Yu, H., Chen, H., Zhao, Y., Yuan, X., Chu, W., Li, H., 2022. Near-Infrared Light Responsive TiO2 for Efficient Solar Energy Utilization. Advanced Functional Materials 32 (12), 2108977. https://doi.org/10.1002/ADFM.202108977.

Jo, W.K., Natarajan, T.S., 2015. Influence of TiO2 morphology on the photocatalytic efficiency of direct Z-scheme g-C3N4/TiO2 photocatalysts for isoniazid degradation. Chemical Engineering Journal 281, 549–565. https://doi.org/10.1016/J.CEJ.2015.06.120.

John, P., Johari, K., Gnanasundaram, N., Appusamy, A., Thanabalan, M., 2021. Enhanced photocatalytic performance of visible light driven TiO2/g-C3N4 for degradation of diclofenac in aqueous solution. Environmental Technology & Innovation 22, 101412. https://doi.org/10.1016/J.ETI.2021.101412.

Kamil, A.M., Mohammed, H.T., Balakit, A.A., Hussein, F.H., Bahnemann, D.W., El-Hiti, G.A., 2018. Synthesis, Characterization and Photocatalytic Activity of Carbon Nanotube/Titanium Dioxide Nanocomposites. Arab J Sci Eng 43 (1), 199–210.

Khan, S.A., Arshad, Z., Shahid, S., Arshad, I., Rizwan, K., Sher, M., Fatima, U., 2019. Synthesis of TiO2/Graphene oxide nanocomposites for their enhanced photocatalytic activity against methylene blue dye and ciprofloxacin. Composites Part B: Engineering 175, 107120. https://doi.org/10.1016/J.COMPOSITESB.2019.107120.

Kuldeep, A.R., Dhabbe, R.S., Garadkar, K.M., 2021. Development of g-C3N4-TiO2 visible active hybrid photocatalyst for the photodegradation of methyl orange. Res Chem Intermed 47 (12), 5155–5174.

Kumar, S.G., Devi, L.G., 2011. Review on Modified TiO2 Photocatalysis under UV/Visible Light: Selected Results and Related Mechanisms on Interfacial Charge Carrier Transfer Dynamics. Journal of Physical Chemistry A 115 (46), 13211–13241. https://doi.org/10.1021/JP204364A.

Kumar, M., Nandi, M., Pakshirajan, K., 2021. Recent advances in heavy metal recovery from wastewater by biogenic sulfide precipitation. Journal of Environmental Management 278, 111555. https://doi.org/10.1016/J.JENVMAN.2020.111555.

Kuvarega, A.T., Mamba, B.B., 2016. Double Walled Carbon Nanotube/TiO2 Nanocomposites for Photocatalytic Dye Degradation. Journal of Nanomaterials 2016, 1–9.

Leary, R., Westwood, A., 2011. Carbonaceous nanomaterials for the enhancement of TiO2 photocatalysis. Carbon 49 (3), 741–772. https://doi.org/10.1016/J.CARBON.2010.10.010.

Lettmann, C., Hildenbrand, K., Kisch, H., Macyk, W., Maier, W.F., 2001. Visible light photodegradation of 4-chlorophenol with a coke-containing titanium dioxide photocatalyst. Applied Catalysis B: Environmental 32 (4), 215–227. https://doi.org/10.1016/S0926-3373(01)00141-2.

Li, P., Yang, C., Sun, F., Li, X., yan., 2021. Fabrication of conductive ceramic membranes for electrically assisted fouling control during membrane filtration for wastewater treatment. Chemosphere 280, 130794. https://doi.org/10.1016/J.CHEMOSPHERE.2021.130794.

Li, Q., Zong, L., Xing, Y., Wang, X., Yu, L., Yang, J., 2013. Preparation of g-C3N4/TiO2 nanocomposites and investigation of their photocatalytic activity. Science of Advanced Materials 5 (9), 1316–1322. https://doi.org/10.1166/SAM.2013.1589.

Liao, G., Gong, Y., Zhang, L., Gao, H., Yang, G.J., Fang, B., 2019. Semiconductor polymeric graphitic carbon nitride photocatalysts: the "holy grail" for the photocatalytic hydrogen evolution reaction under visible light. Energy & Environmental Science 12 (7), 2080–2147. https://doi.org/10.1039/C9EE00717B.

Liao, W., Murugananthan, M., Zhang, Y., 2015. Synthesis of Z-scheme g-C3N4–Ti3+/TiO2 material: an efficient visible light photoelectrocatalyst for degradation of phenol. Physical Chemistry Chemical Physics 17 (14), 8877–8884. https://doi.org/10.1039/C5CP00639B.

Liao, M., Su, L., Deng, Y., Xiong, S., Tang, R., Wu, Z., Ding, C., Yang, L., Gong, D., 2021. Strategies to improve WO3-based photocatalysts for wastewater treatment: a review. J Mater Sci 56 (26), 14416–14447.

Lim, T.-T., Yap, P.-S., Srinivasan, M., Fane, A.G., 2011. TiO 2/AC Composites for Synergistic Adsorption-Photocatalysis Processes: Present Challenges and Further Developments for Water Treatment and Reclamation. Critical Reviews in Environmental Science and Technology 41 (13), 1173–1230.

Ling, L., Wang, C., Ni, M., Shang, C., 2016. Enhanced photocatalytic activity of TiO2/single-walled carbon nanotube (SWCNT) composites under UV-A irradiation. Separation and Purification Technology 169, 273–278. https://doi.org/10.1016/J.SEPPUR.2016.05.051.

Liu, F., Chung, S., Oh, G., Seo, T.S., 2012. Three-dimensional graphene oxide nanostructure for fast and efficient water-soluble dye removal. ACS Applied Materials and Interfaces 4 (2), 922–927. https://doi.org/10.1021/AM201590Z/SUPPL_FILE/AM201590Z_SI_001.PDF.

Liu, Q., Fan, C., Tang, H., Sun, X., Yang, J., Cheng, X., 2015. One-pot synthesis of g-C3N4/V2O5 composites for visible light-driven photocatalytic activity. Applied Surface Science 358, 188–195. https://doi.org/10.1016/J.APSUSC.2015.09.010.

Liu, X., Yang, W., Yu, C., Zhang, H., 2018. Influence of TiO2 morphology on adsorption-photocatalytic efficiency of TiO2-graphene composites for methylene blue degradation. Journal of Environmental Chemical Engineering 6 (4), 4899–4907. https://doi.org/10.1016/J.JECE.2018.07.009.

Liu, S., Yu, J., Jaroniec, M., 2010. Tunable photocatalytic selectivity of hollow TiO2 microspheres composed of anatase polyhedra with exposed 001 facets. Journal of the American Chemical Society 132 (34), 11914–11916. https://doi.org/10.1021/JA105283S/SUPPL_FILE/JA105283S_SI_001.PDF.

Liu, H., Yu, D., Sun, T., Du, H., Jiang, W., Muhammad, Y., Huang, L., 2019. Fabrication of surface alkalinized g-C3N4 and TiO2 composite for the synergistic adsorption-photocatalytic degradation of methylene blue. Applied Surface Science 473, 855–863. https://doi.org/10.1016/J.APSUSC.2018.12.162.

Lu, D., Fang, P., Wu, W., Ding, J., Jiang, L., Zhao, X., Li, C., Yang, M., Li, Y., Wang, D., 2017. Solvothermal-assisted synthesis of self-assembling TiO2 nanorods on large graphitic carbon nitride sheets with their anti-recombination in the photocatalytic removal of Cr(VI) and rhodamine B under visible light irradiation. Nanoscale 9 (9), 3231–3245. https://doi.org/10.1039/C6NR09137G.

Luo, X., Liang, C., & Hu, Y. (2019). Comparison of Different Enhanced Coagulation Methods for Azo Dye Removal from Wastewater. *Sustainability 2019, Vol. 11, Page 4760*, *11*(17), 4760. https://doi.org/10.3390/SU11174760.

Lv, R., Cruz-Silva, E., Terrones, M., 2014. Building complex hybrid carbon architectures by covalent interconnections: Graphene-nanotube hybrids and more. ACS Nano 8 (5), 4061–4069. https://doi.org/10.1021/NN502426C/ASSET/IMAGES/NN502426C.SOCIAL.JPEG_V03.

Ma, L., Wang, G., Jiang, C., Bao, H., Xu, Q., 2018. Synthesis of core-shell TiO2@g-C3N4 hollow microspheres for efficient photocatalytic degradation of rhodamine B under visible light. Applied Surface Science 430, 263–272. https://doi.org/10.1016/J.APSUSC.2017.07.282.

Ma, D., Yi, H., Lai, C., Liu, X., Huo, X., An, Z., Li, L., Fu, Y., Li, B., Zhang, M., Qin, L., Liu, S., Yang, L., 2021. Critical review of advanced oxidation processes in organic wastewater treatment. Chemosphere 275, 130104. https://doi.org/10.1016/J.CHEMOSPHERE.2021.130104.

Maeng, S.K., Cho, K., Jeong, B., Lee, J., Lee, Y., Lee, C., Choi, K.J., Hong, S.W., 2015. Substrate-immobilized electrospun TiO2 nanofibers for photocatalytic degradation of pharmaceuticals: The effects of pH and dissolved organic matter characteristics. Water Research 86, 25–34. https://doi.org/10.1016/J.WATRES.2015.05.032.

Martins, A.C., Cazetta, A.L., Pezoti, O., Souza, J.R.B., Zhang, T., Pilau, E.J., Asefa, T., Almeida, V.C., 2017. Sol-gel synthesis of new TiO2/activated carbon photocatalyst and its application for degradation of tetracycline. Ceramics International 43 (5), 4411–4418. https://doi.org/10.1016/J.CERAMINT.2016.12.088.

Martins, P.M., Ferreira, C.G., Silva, A.R., Magalhães, B., Alves, M.M., Pereira, L., Marques, P.A.A.P., Melle-Franco, M., Lanceros-Méndez, S., 2018. TiO2/graphene and TiO2/graphene oxide nanocomposites for photocatalytic applications: A computer modeling and experimental study. Composites Part B: Engineering 145, 39–46. https://doi.org/10.1016/J.COMPOSITESB.2018.03.015.

Mathew, S., Ganguly, P., Rhatigan, S., Kumaravel, V., Byrne, C., Hinder, S., Bartlett, J., Nolan, M., Pillai, S., 2018. Cu-Doped TiO2: Visible Light Assisted Photocatalytic Antimicrobial Activity. Applied Sciences 8 (11), 2067. https://doi.org/10.3390/app8112067.

Minella, M., Sordello, F., Minero, C., 2017. Photocatalytic process in TiO2/graphene hybrid materials. Evidence of charge separation by electron transfer from reduced graphene oxide to TiO2. Catalysis Today 281, 29–37. https://doi.org/10.1016/J.CATTOD.2016.03.040.

Miranda, C., Mansilla, H., Yáñez, J., Obregón, S., Colón, G., 2013. Improved photocatalytic activity of g-C3N4/TiO2 composites prepared by a simple impregnation method. Journal of Photochemistry and Photobiology A: Chemistry 253, 16–21.

Mohini, R., Lakshminarasimhan, N., 2016. Coupled semiconductor nanocomposite g-C3N4/TiO2 with enhanced visible light photocatalytic activity. Materials Research Bulletin 76, 370–375. https://doi.org/10.1016/J.MATERRESBULL.2015.12.034.

Monga, D., Basu, S., 2019. Enhanced photocatalytic degradation of industrial dye by g-C3N4/TiO2 nanocomposite: Role of shape of TiO2. Advanced Powder Technology 30 (5), 1089–1098. https://doi.org/10.1016/J.APT.2019.03.004.

Murgolo, S., Petronella, F., Ciannarella, R., Comparelli, R., Agostiano, A., Curri, M.L., Mascolo, G., 2015. UV and solar-based photocatalytic degradation of organic pollutants by nano-sized TiO2 grown on carbon nanotubes. Catalysis Today 240 (PA), 114–124. https://doi.org/10.1016/J.CATTOD.2014.04.021.

Mutuma, B.K., Shao, G.N., Kim, W.D., Kim, H.T., 2015. Sol–gel synthesis of mesoporous anatase–brookite and anatase–brookite–rutile TiO2 nanoparticles and their photocatalytic properties. Journal of Colloid and Interface Science 442, 1–7. https://doi.org/10.1016/J.JCIS.2014.11.060.

Najafi, M., Kermanpur, A., Rahimipour, M.R., Najafizadeh, A., 2017. Effect of TiO2 morphology on structure of TiO2-graphene oxide nanocomposite synthesized via a one-step hydrothermal method. Journal of Alloys and Compounds 722, 272–277. https://doi.org/10.1016/J.JALLCOM.2017.06.001.

Nasr, C., Vinodgopal, K., Fisher, L., Hotchandani, S., Chattopadhyay, A.K., Kamat, P.V., 1996. Environmental Photochemistry on Semiconductor Surfaces. Visible Light Induced Degradation of a Textile Diazo Dye, Naphthol Blue Black, on TiO2 Nanoparticles. Journal of Physical Chemistry 100 (20), 8436–8442. https://doi.org/10.1021/JP953556V.

Natarajan, T.S., Lee, J.Y., Bajaj, H.C., Jo, W.K., Tayade, R.J., 2017. Synthesis of multiwall carbon nanotubes/TiO2 nanotube composites with enhanced photocatalytic decomposition efficiency. Catalysis Today 282, 13–23. https://doi.org/10.1016/J.CATTOD.2016.03.018.

Natarajan, T.S., Gopi, P.K., Natarajan, K., Bajaj, H.C., Tayade, R.J., 2021. TiO2/graphene oxide nanocomposite with enhanced photocatalytic capacity for degradation of 2,4-dichlorophenoxyacetic acid herbicide. Water-Energy Nexus 4, 103–112. https://doi.org/10.1016/J.WEN.2021.07.001.

Niazi, Z., Goharshadi, E.K., Mashreghi, M., Jorabchi, M.N., 2021. Highly efficient solar photocatalytic degradation of a textile dye by TiO2/graphene quantum dots nanocomposite. Photochemical and Photobiological Sciences 20 (1), 87–99. https://doi.org/10.1007/S43630-020-00005-7/FIGURES/6.

Omri, A., Benzina, M., 2014. Almond shell activated carbon: adsorbent and catalytic support in the phenol degradation. Environ Monit Assess 186 (6), 3875–3890.

Ong, W.J., Tan, L.L., Ng, Y.H., Yong, S.T., Chai, S.P., 2016. Graphitic Carbon Nitride (g-C3N4)-Based Photocatalysts for Artificial Photosynthesis and Environmental Remediation: Are We a Step Closer To Achieving Sustainability? Chemical Reviews 116 (12), 7159–7329. https://doi.org/10.1021/ACS.CHEMREV.6B00075.

Park, C.H., Lee, C.M., Choi, J.W., Park, G.C., Joo, J., 2018. Enhanced photocatalytic activity of porous single crystal TiO2/CNT composites by annealing process. Ceramics International 44 (2), 1641–1645. https://doi.org/10.1016/J.CERAMINT.2017.10.086.

Paumo, H.K., Dalhatou, S., Katata-Seru, L.M., Kamdem, B.P., Tijani, J.O., Vishwanathan, V., Kane, A., Bahadur, I., 2021. TiO2 assisted photocatalysts for degradation of emerging organic pollutants in water and wastewater. Journal of Molecular Liquids 331, 115458. https://doi.org/10.1016/J.MOLLIQ.2021.115458.

Peñas-Garzón, Manuel, Gómez-Avilés, A., Bedia, J., Rodriguez, J. J., & Belver, C. (2019). Effect of Activating Agent on the Properties of TiO2/Activated Carbon Heterostructures for Solar Photocatalytic Degradation of Acetaminophen. *Materials 2019, Vol. 12, Page 378*, *12*(3), 378. https://doi.org/10.3390/MA12030378.

Peñas-Garzón, M., Gómez-Avilés, A., Belver, C., Rodriguez, J.J., Bedia, J., 2020. Degradation pathways of emerging contaminants using TiO2-activated carbon heterostructures in aqueous solution under simulated solar light. Chemical Engineering Journal 392, 124867. https://doi.org/10.1016/J.CEJ.2020.124867.

Perera, S.D., Mariano, R.G., Vu, K., Nour, N., Seitz, O., Chabal, Y., Balkus, K.J., 2012. Hydrothermal synthesis of graphene-TiO 2 nanotube composites with enhanced photocatalytic activity. ACS Catalysis 2 (6), 949–956. https://doi.org/10.1021/CS200621C/SUPPL_FILE/CS200621C_SI_001.PDF.

Piątkowska, A., Janus, M., Szymański, K., & Mozia, S. (2021). C-,N- and S-Doped TiO2 Photocatalysts: A Review. *Catalysts 2021, Vol. 11, Page 144*, *11*(1), 144. https://doi.org/10.3390/CATAL11010144.

Prashad Ojha, D., Babu Poudel, M., Joo Kim, H., 2020. Investigation of electrochemical performance of a high surface area mesoporous Mn doped TiO2 nanoparticle for a supercapacitor. Materials Letters 264, 127363. https://doi.org/10.1016/J.MATLET.2020.127363.

Qi, F., An, W., Wang, H., Hu, J., Guo, H., Liu, L., Cui, W., 2020. Combing oxygen vacancies on TiO2 nanorod arrays with g-C3N4 nanosheets for enhancing photoelectrochemical degradation of phenol. Materials Science in Semiconductor Processing 109, 104954. https://doi.org/10.1016/J.MSSP.2020.104954.

Qu, X., Chen, C., Lin, J., Qiang, W., Zhang, L., Sun, D., 2022. Engineered defect-rich TiO2/g-C3N4 heterojunction: A visible light-driven photocatalyst for efficient degradation of phenolic wastewater. Chemosphere 286, 131696. https://doi.org/10.1016/J.CHEMOSPHERE.2021.131696.

Raja, A., Selvakumar, K., Rajasekaran, P., Arunpandian, M., Ashokkumar, S., Kaviyarasu, K., Asath Bahadur, S., Swaminathan, M., 2019. Visible active reduced graphene oxide loaded titania for photodecomposition of ciprofloxacin and its antibacterial activity. Colloids and Surfaces A: Physicochemical and Engineering Aspects 564, 23–30. https://doi.org/10.1016/J.COLSURFA.2018.12.024.

Rashid, R., Shafiq, I., Akhter, P., Iqbal, M.J., Hussain, M., 2021. A state-of-the-art review on wastewater treatment techniques: the effectiveness of adsorption method. Environ Sci Pollut Res 28 (8), 9050–9066.

Rastogi, M., Kushwaha, H.S., Vaish, R., 2016. Highly efficient visible light mediated azo dye degradation through barium titanate decorated reduced graphene oxide sheets. Electron. Mater. Lett. 12 (2), 281–289.

Reddy, K.R., Reddy, C.V., Nadagouda, M.N., Shetti, N.P., Jaesool, S., Aminabhavi, T.M., 2019. Polymeric graphitic carbon nitride (g-C3N4)-based semiconducting nanostructured materials: Synthesis methods, properties and photocatalytic applications. Journal of Environmental Management 238, 25–40. https://doi.org/10.1016/J.JENVMAN.2019.02.075.

Ren, Y., Zeng, D., Ong, W.J., 2019. Interfacial engineering of graphitic carbon nitride (g-C3N4)-based metal sulfide heterojunction photocatalysts for energy conversion: A review. Chinese Journal of Catalysis 40 (3), 289–319. https://doi.org/10.1016/S1872-2067(19)63293-6.

Rong, X., Qiu, F., Zhang, C., Fu, L., Wang, Y., Yang, D., 2015. Preparation, characterization and photocatalytic application of TiO2–graphene photocatalyst under visible light irradiation. Ceramics International 41 (2), 2502–2511. https://doi.org/10.1016/J.CERAMINT.2014.10.072.

Roushani, M., Mavaei, M., Rajabi, H.R., 2015. Graphene quantum dots as novel and green nano-materials for the visible-light-driven photocatalytic degradation of cationic dye. Journal of Molecular Catalysis A: Chemical 409, 102–109. https://doi.org/10.1016/J.MOLCATA.2015.08.011.

Saleh, I.A., Zouari, N., Al-Ghouti, M.A., 2020. Removal of pesticides from water and wastewater: Chemical, physical and biological treatment approaches. Environmental Technology & Innovation 19, 101026. https://doi.org/10.1016/J.ETI.2020.101026.

Sampaio, M.J., Benyounes, A., Serp, P., Faria, J.L., Silva, C.G., 2018. Photocatalytic synthesis of vanillin using N-doped carbon nanotubes/ZnO catalysts under UV-LED irradiation. Applied Catalysis A: General 551, 71–78. https://doi.org/10.1016/J.APCATA.2017.12.002.

Seza, A., Soleimani, F., Naseri, N., Soltaninejad, M., Montazeri, S.M., Sadrnezhaad, S.K., Mohammadi, M.R., Moghadam, H.A., Forouzandeh, M., Amin, M.H., 2018. Novel microwave-assisted synthesis of porous g-C3N4/SnO2 nanocomposite for solar water-splitting. Applied Surface Science 440, 153–161. https://doi.org/10.1016/J.APSUSC.2018.01.133.

Shaban, M., Ashraf, A.M., Abukhadra, M.R., 2018. TiO2 Nanoribbons/Carbon Nanotubes Composite with Enhanced Photocatalytic Activity; Fabrication, Characterization, and Application. Sci Rep 8 (1).

Sharma, P., Pandey, A.K., Kim, S.H., Singh, S.P., Chaturvedi, P., Varjani, S., 2021a. Critical review on microbial community during in-situ bioremediation of heavy metals from industrial wastewater. Environmental Technology & Innovation 24, 101826. https://doi.org/10.1016/J.ETI.2021.101826.

Sharma, H.K., Sharma, S.K., Vemula, K., Koirala, A.R., Yadav, H.M., Singh, B.P., 2021b. CNT facilitated interfacial charge transfer of TiO2 nanocomposite for controlling the electron-hole recombination. Solid State Sciences 112, 106492. https://doi.org/10.1016/J.SOLIDSTATESCIENCES.2020.106492.

Sharma, M., Vaidya, S., Ganguli, A.K., 2017. Enhanced photocatalytic activity of g-C3N4-TiO2 nanocomposites for degradation of Rhodamine B dye. Journal of Photochemistry and Photobiology A: Chemistry 335, 287–293. https://doi.org/10.1016/J.JPHOTOCHEM.2016.12.002.

Shen, L., Xing, Z., Zou, J., Li, Z., Wu, X., Zhang, Y., Zhu, Q., Yang, S., & Zhou, W. (2017). Black TiO2 nanobelts/g-C3N4 nanosheets Laminated Heterojunctions with Efficient Visible-Light-Driven Photocatalytic Performance. *Scientific Reports 2017 7:1*, *7*(1), 1–11. https://doi.org/10.1038/srep41978.

Slimen, H., Houas, A., Nogier, J.P., 2011. Elaboration of stable anatase TiO2 through activated carbon addition with high photocatalytic activity under visible light. Journal of Photochemistry and Photobiology A: Chemistry 221 (1), 13–21. https://doi.org/10.1016/J.JPHOTOCHEM.2011.04.013.

Song, C., Chen, P., Wang, C., Zhu, L., 2012. Photodegradation of perfluorooctanoic acid by synthesized TiO2–MWCNT composites under 365 nm UV irradiation. Chemosphere 86 (8), 853–859. https://doi.org/10.1016/J.CHEMOSPHERE.2011.11.034.

Sutar, R.S., Barkul, R.P., Delekar, S.D., Patil, M.K., 2020. Sunlight assisted photocatalytic degradation of organic pollutants using g-C3N4-TiO2 nanocomposites. Arabian Journal of Chemistry 13 (4), 4966–4977. https://doi.org/10.1016/J.ARABJC.2020.01.019.

Tao, X., Hu, X., Wen, Z., Ming, Y., Li, J., Liu, Y., Chen, R., 2022. Highly efficient Cr(VI) removal from industrial electroplating wastewater over Bi2S3 nanostructures prepared by dual sulfur-precursors: Insights on the promotion effect of sulfate ions. Journal of Hazardous Materials 424, 127423. https://doi.org/10.1016/J.JHAZMAT.2021.127423.

Thambiliyagodage, C., 2021. Activity enhanced TiO2 nanomaterials for photodegradation of dyes – A review. Environmental Nanotechnology, Monitoring & Management 16, 100592. https://doi.org/10.1016/J.ENMM.2021.100592.

Thambiliyagodage, C., & Mirihana, S. (2021). Photocatalytic activity of Fe and Cu co-doped TiO2 nanoparticles under visible light. *Journal of Sol-Gel Science and Technology 2021 99:1*, *99*(1), 109–121. https://doi.org/10.1007/S10971-021-05556-4.

Thambiliyagodage, C., Usgodaarachchi, L., 2021. Photocatalytic activity of N, Fe and Cu co-doped TiO2 nanoparticles under sunlight. Current Research in Green and Sustainable Chemistry 4, 100186. https://doi.org/10.1016/J.CRGSC.2021.100186.

Toghan, A., Abd El-Lateef, H.M., Taha, K.K., Modwi, A., 2021. Mesoporous TiO2@g-C3N4 composite: construction, characterization, and boosting indigo carmine dye destruction. Diamond and Related Materials 118, 108491. https://doi.org/10.1016/J.DIAMOND.2021.108491.

Ton, N.N.T., Dao, A.T.N., Kato, K., Ikenaga, T., Trinh, D.X., Taniike, T., 2018. One-pot synthesis of TiO2/graphene nanocomposites for excellent visible light photocatalysis based on chemical exfoliation method. Carbon 133, 109–117. https://doi.org/10.1016/J.CARBON.2018.03.025.

Trapalis, A., Todorova, N., Giannakopoulou, T., Boukos, N., Speliotis, T., Dimotikali, D., Yu, J., 2016. TiO2/graphene composite photocatalysts for NOx removal: A comparison of surfactant-stabilized graphene and reduced graphene oxide. Applied Catalysis B: Environmental 180, 637–647. https://doi.org/10.1016/J.APCATB.2015.07.009.

Tryba, B., Morawski, A.W., Inagaki, M., 2003. Application of TiO2-mounted activated carbon to the removal of phenol from water. Applied Catalysis B: Environmental 41 (4), 427–433. https://doi.org/10.1016/S0926-3373(02)00173-X.

Usgodaarachchi, L., Thambiliyagodage, C., Wijesekera, R., Bakker, M.G., 2021. Synthesis of mesoporous silica nanoparticles derived from rice husk and surface-controlled amine functionalization for efficient adsorption of methylene blue from aqueous solution. Current Research in Green and Sustainable Chemistry 4, 100116. https://doi.org/10.1016/J.CRGSC.2021.100116.

Varnagiris, S., Medvids, A., Lelis, M., Milcius, D., Antuzevics, A., 2019. Black carbon-doped TiO2 films: Synthesis, characterization and photocatalysis. Journal of Photochemistry and Photobiology A: Chemistry 382, 111941. https://doi.org/10.1016/J.JPHOTOCHEM.2019.111941.

Vaziri, H.S., Shokuhfar, A., Salman, S., Afghahi, S., 2021. The role of surfactant to enhance photocatalyst performance on phenol degradation in TiO2-CNT composite-modified CNT (Cetyltrimethylammonium bromide). IOP Conference Series: Materials Science and Engineering 1041 (1), 012048. https://doi.org/10.1088/1757-899X/1041/1/012048.

Wang, C., Cao, M., Wang, P., Ao, Y., Hou, J., Qian, J., 2014. Preparation of graphene–carbon nanotube–TiO2 composites with enhanced photocatalytic activity for the removal of dye and Cr (VI). Applied Catalysis A: General 473, 83–89. https://doi.org/10.1016/J.APCATA.2013.12.028.

Wang, M., Cui, S., Yang, X., Bi, W., 2015. Synthesis of g-C3N4/Fe3O4 nanocomposites and application as a new sorbent for solid phase extraction of polycyclic aromatic hydrocarbons in water samples. Talanta 132, 922–928. https://doi.org/10.1016/J.TALANTA.2014.08.071.

Wang, Xinchen, Maeda, K., Thomas, A., Takanabe, K., Xin, G., Carlsson, J. M., Domen, K., & Antonietti, M. (2008). A metal-free polymeric photocatalyst for hydrogen production from water under visible light. *Nature Materials 2009 8:1*, *8*(1), 76–80. https://doi.org/10.1038/nmat2317.

Wang, L., Guo, J., Dang, J., Huang, X., Chen, S., Guan, W., 2018a. Comparison of the photocatalytic performance of TiO2/AC and TiO2/CNT nanocomposites for methyl orange photodegradation. Water Science and Technology 78 (5), 1082–1093. https://doi.org/10.2166/WST.2018.374.

Wang, X., Hu, Z., Chen, Y., Zhao, G., Liu, Y., Wen, Z., 2009. A novel approach towards high-performance composite photocatalyst of TiO2 deposited on activated carbon. Applied Surface Science 255 (7), 3953–3958. https://doi.org/10.1016/J.APSUSC.2008.10.083.

Wang, H., Liang, Y., Liu, L., Hu, J., Cui, W., 2018b. Highly ordered TiO2 nanotube arrays wrapped with g-C3N4 nanoparticles for efficient charge separation and increased photoelectrocatalytic degradation of phenol. Journal of Hazardous Materials 344, 369–380. https://doi.org/10.1016/J.JHAZMAT.2017.10.044.

Wang, S., Liang, F., Li, S., Tian, L., Zhang, S., Jia, Q., Chang, S., Yan, S., Zhang, H., 2021. Synthesis of monophase two-dimensional α-Si3N4 nanoplatelets via an ionothermal route. International Journal of Applied Ceramic Technology 18 (4), 1183–1191. https://doi.org/10.1111/IJAC.13776.

Wang, Y., Roddick, F.A., Fan, L., 2017. Direct and indirect photolysis of seven micropollutants in secondary effluent from a wastewater lagoon. Chemosphere 185, 297–308. https://doi.org/10.1016/J.CHEMOSPHERE.2017.06.122.

Wang, W., Silva, C.G., Faria, J.L., 2007. Photocatalytic degradation of Chromotrope 2R using nanocrystalline TiO2/activated-carbon composite catalysts. Applied Catalysis B: Environmental 70 (1–4), 470–478. https://doi.org/10.1016/J.APCATB.2005.11.034.

Wang, X., Wang, F., Bo, C., Cheng, K., Wang, J., Zhang, J., Song, H., 2018c. Promotion of phenol photodecomposition and the corresponding decomposition mechanism over g-C3N4/TiO2 nanocomposites. Applied Surface Science 453, 320–329. https://doi.org/10.1016/J.APSUSC.2018.05.082.

Wang, F., Zhang, K., 2011. Reduced graphene oxide–TiO2 nanocomposite with high photocatalystic activity for the degradation of rhodamine B. Journal of Molecular Catalysis A: Chemical 345 (1–2), 101–107. https://doi.org/10.1016/J.MOLCATA.2011.05.026.

Wei, Z., Liang, F., Liu, Y., Luo, W., Wang, J., Yao, W., Zhu, Y., 2017a. Photoelectrocatalytic degradation of phenol-containing wastewater by TiO2/g-C3N4 hybrid heterostructure thin film. Applied Catalysis B: Environmental 201, 600–606. https://doi.org/10.1016/J.APCATB.2016.09.003.

Wei, H., McMaster, W.A., Tan, J.Z.Y., Cao, L., Chen, D., Caruso, R.A., 2017b. Mesoporous TiO2/g-C3N4 Microspheres with Enhanced Visible-Light Photocatalytic Activity. Journal of Physical Chemistry C 121 (40), 22114–22122. https://doi.org/10.1021/ACS.JPCC.7B06493/SUPPL_FILE/JP7B06493_SI_001.PDF.

Wen, J., Xie, J., Chen, X., Li, X., 2017. A review on g-C3N4-based photocatalysts. Applied Surface Science 391, 72–123. https://doi.org/10.1016/J.APSUSC.2016.07.030.

Wong, J.K.H., Tan, H.K., Lau, S.Y., Yap, P.S., Danquah, M.K., 2019. Potential and challenges of enzyme incorporated nanotechnology in dye wastewater treatment: A review. Journal of Environmental Chemical Engineering 7 (4), 103261. https://doi.org/10.1016/J.JECE.2019.103261.

Xaba, T., 2021. Green synthesis of ZnS nanoparticles and fabrication of ZnS-chitosan nanocomposites for the removal of Cr(vi) ion from wastewater. Green Processing and Synthesis 10 (1), 374–383. https://doi.org/10.1515/GPS-2021-0026/MACHINEREADABLECITATION/RIS.

Xing, B., Shi, C., Zhang, C., Yi, G., Chen, L., Guo, H., Huang, G., Cao, J., 2016. Preparation of TiO2/Activated Carbon Composites for Photocatalytic Degradation of RhB under UV Light Irradiation. Journal of Nanomaterials 2016. https://doi.org/10.1155/2016/8393648.

Xu, J., Brenner, T.J.K., Chabanne, L., Neher, D., Antonietti, M., Shalom, M., 2014. Liquid-based growth of polymeric carbon nitride layers and their use in a mesostructured polymer solar cell with v oc exceeding 1 v. Journal of the American Chemical Society 136 (39), 13486–13489. https://doi.org/10.1021/JA508329C/SUPPL_FILE/JA508329C_SI_001.PDF.

Xu, J., Wang, G., Fan, J., Liu, B., Cao, S., Yu, J., 2015. g-C3N4 modified TiO2 nanosheets with enhanced photoelectric conversion efficiency in dye-sensitized solar cells. Journal of Power Sources 274, 77–84. https://doi.org/10.1016/J.JPOWSOUR.2014.10.033.

Xue, G., Liu, H., Chen, Q., Hills, C., Tyrer, M., Innocent, F., 2011. Synergy between surface adsorption and photocatalysis during degradation of humic acid on TiO2/activated carbon composites. Journal of Hazardous Materials 186 (1), 765–772. https://doi.org/10.1016/J.JHAZMAT.2010.11.063.

Yang, X.J., Wang, S., Sun, H.M., Wang, X.B., Lian, J.S., 2015. Preparation and photocatalytic performance of Cu-doped TiO2 nanoparticles. Transactions of Nonferrous Metals Society of China 25 (2), 504–509. https://doi.org/10.1016/S1003-6326(15)63631-7.

Yang, J., Wang, H., Jiang, L., Yu, H., Zhao, Y., Chen, H., Yuan, X., Liang, J., Li, H., Wu, Z., 2022. Defective polymeric carbon nitride: Fabrications, photocatalytic applications and perspectives. Chemical Engineering Journal 427, 130991. https://doi.org/10.1016/J.CEJ.2021.130991.

Yang, K., Xing, B., 2009. Adsorption of fulvic acid by carbon nanotubes from water. Environmental Pollution 157 (4), 1095–1100. https://doi.org/10.1016/J.ENVPOL.2008.11.007.

Ye, S., Qiu, L.G., Yuan, Y.P., Zhu, Y.J., Xia, J., Zhu, J.F., 2013. Facile fabrication of magnetically separable graphitic carbon nitride photocatalysts with enhanced photocatalytic activity under visible light. Journal of Materials Chemistry A 1 (9), 3008–3015. https://doi.org/10.1039/C2TA01069K.

Yong, X., Schoonen, M.A.A., 2000. The absolute energy positions of conduction and valence bands of selected semiconducting minerals. American Mineralogist 85 (3–4), 543–556. https://doi.org/10.2138/AM-2000-0416.

Yu, Q., Deng, S., Yu, G., 2008. Selective removal of perfluorooctane sulfonate from aqueous solution using chitosan-based molecularly imprinted polymer adsorbents. Water Research 42 (12), 3089–3097. https://doi.org/10.1016/J.WATRES.2008.02.024.

Yu, J., Wang, S., Low, J., Xiao, W., 2013. Enhanced photocatalytic performance of direct Z-scheme g-C3N4–TiO2 photocatalysts for the decomposition of formaldehyde in air. Physical Chemistry Chemical Physics 15 (39), 16883–16890. https://doi.org/10.1039/C3CP53131G.

Zang, Y., Li, L., Li, X., Lin, R., Li, G., 2014. Synergistic collaboration of g-C3N4/SnO2 composites for enhanced visible-light photocatalytic activity. Chemical Engineering Journal 246, 277–286. https://doi.org/10.1016/J.CEJ.2014.02.068.

Zazo, J.A., Bedia, J., Fierro, C.M., Pliego, G., Casas, J.A., Rodriguez, J.J., 2012. Highly stable Fe on activated carbon catalysts for CWPO upon FeCl3 activation of lignin from black liquors. Catalysis Today 187 (1), 115–121. https://doi.org/10.1016/J.CATTOD.2011.10.003.

Zeng, D., Zhou, T., Ong, W.J., Wu, M., Duan, X., Xu, W., Chen, Y., Zhu, Y.A., Peng, D.L., 2019. Sub-5 nm Ultra-Fine FeP Nanodots as Efficient Co-Catalysts Modified Porous g-C3N4for Precious-Metal-Free Photocatalytic Hydrogen Evolution under Visible Light. ACS Applied Materials and Interfaces 11 (6), 5651–5660. https://doi.org/10.1021/ACSAMI.8B20958/SUPPL_FILE/AM8B20958_SI_001.PDF.

Zhang, Hao, Lv, X., Li, Y., Wang, Y., & Li, J. (2010). P25-graphene composite as a high performance photocatalyst. *ACS Nano*, *4*(1), 380–386. https://doi.org/10.1021/NN901221K/SUPPL_FILE/NN901221K_SI_001.PDF.

Zhang, N., Gao, J., Huang, C., Liu, W., Tong, P., Zhang, L., 2016. In situ hydrothermal growth of ZnO/g-C3N4 nanoflowers coated solid-phase microextraction fibers coupled with GC-MS for determination of pesticides residues. Analytica Chimica Acta 934, 122–131. https://doi.org/10.1016/J.ACA.2016.06.029.

Zhang, X., He, S., Jiang, S.P., 2020. WOx/g-C3N4 layered heterostructures with controlled crystallinity towards superior photocatalytic degradation and H2 generation. Carbon 156, 488–498. https://doi.org/10.1016/J.CARBON.2019.09.083.

Zhang, J., Sun, J., Maeda, K., Domen, K., Liu, P., Antonietti, M., Fu, X., Wang, X., 2011. Sulfur-mediated synthesis of carbon nitride: Band-gap engineering and improved functions for photocatalysis. Energy & Environmental Science 4 (3), 675–678. https://doi.org/10.1039/C0EE00418A.

Zhang, H., Wang, Z., Li, R., Guo, J., Li, Y., Zhu, J., Xie, X., 2017. TiO2 supported on reed straw biochar as an adsorptive and photocatalytic composite for the efficient degradation of sulfamethoxazole in aqueous matrices. Chemosphere 185, 351–360. https://doi.org/10.1016/J.CHEMOSPHERE.2017.07.025.

Zhang, Z., Yu, Y., Wang, P., 2012. Hierarchical top-porous/bottom-tubular TiO 2 nanostructures decorated with Pd nanoparticles for efficient photoelectrocatalytic decomposition of synergistic pollutants. ACS Applied Materials and Interfaces 4 (2), 990–996. https://doi.org/10.1021/AM201630S/SUPPL_FILE/AM201630S_SI_001.PDF.

Zhang, X., Zhang, H., Chen, Z., Wei, D., Song, Y., Ma, Y., Zhang, H., 2021. Achieving biogas production and efficient pollutants removal from nitrogenous fertilizer wastewater using combined anaerobic digestion and autotrophic nitrogen removal process. Bioresource Technology 339, 125659. https://doi.org/10.1016/J.BIORTECH.2021.125659.

Zhou, Q., Li, N., Chen, D., Xu, Q., Li, H., He, J., Lu, J., 2022. Efficient removal of Bisphenol A in water via piezocatalytic degradation by equivalent-vanadium-doped SrTiO3 nanofibers. Chemical Engineering Science 247, 116707. https://doi.org/10.1016/J.CES.2021.116707.

Zhou, L., Wang, L., Lei, J., Liu, Y., Zhang, J., 2017. Fabrication of TiO2/Co-g-C3N4 heterojunction catalyst and its photocatalytic performance. Catalysis Communications 89, 125–128. https://doi.org/10.1016/J.CATCOM.2016.09.022.

Zouzelka, R., Kusumawati, Y., Remzova, M., Rathousky, J., Pauporté, T., 2016. Photocatalytic activity of porous multiwalled carbon nanotube-TiO2 composite layers for pollutant degradation. Journal of Hazardous Materials 317, 52–59. https://doi.org/10.1016/J.JHAZMAT.2016.05.056.